Outer Approximation of the Spectrum of a Fractal Laplacian

Tyrus Berry, Steven M. Heilman, and Robert S. Strichartz

CONTENTS

We present a new method to approximate the Neumann spectrum of a Laplacian on a fractal K in the plane as a renormalized limit of the Neumann spectra of the standard Laplacian on a sequence of domains that approximate K from the outside. The method allows a numerical approximation of eigenvalues and eigenfunctions for lower portions of the spectrum. We present experimental evidence that the method works by looking at examples in which the spectrum of the fractal Laplacian is known (the unit interval and the Sierpiński gasket). We also present a speculative description of the spectrum on the standard Sierpiński carpet, where existence of a self-similar Laplacian is known, and also on nonsymmetric and random carpets and the octagasket, where existence of a self-similar Laplacian is not known. At present we have no explanation as to why the method should work. Nevertheless, we are able to prove some new results about the structure of the spectrum involving "miniaturization" of eigenfunctions that we discovered by examining the experimental results obtained using our method.

1. INTRODUCTION

Laplacians arise in many different mathematical contexts, three in particular that will interest us: manifolds, graphs, and fractals. There are connections relating these different types of Laplacians. Manifold Laplacians may be obtained as limits of graph Laplacians for graphs arising from triangulations of the manifold [Colin de Verdière 98, Dodziuk and Patodi 76]. Kigami's approach to constructing Laplacians on certain fractals, such as the Sierpiński gasket (SG), also involves taking limits of graph Laplacians for graphs that approximate the fractal [Kigami 01, Strichartz 99, Strichartz 06]. In this paper we present another connection, whereby we approximate the fractal from without by planar domains and then attempt to capture spectral information about the fractal Laplacian from spectral information about the

2000 AMS Subject Classification: Primary 28A80

Keywords: Fractal, analysis, Laplacian, spectrum, Mandelbrot percolation

1058-6458/2009 $0.50 per page

standard Laplacian on the domains. Thus we add an arrow to the following diagram:

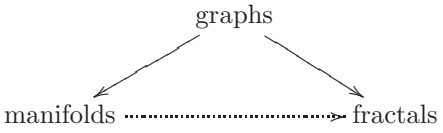

We should point out that the probabilistic approach to constructing Laplacians on fractals also involves approximating from without, but in that case it is the stochastic process generated by the Laplacian that is approximated, so it is not clear how to obtain spectral information.

We may describe our method succinctly as follows. Suppose we have a self-similar fractal K in the plane, determined by the identity

$$K = \bigcup F_i K, \tag{1–1}$$

where $\{F_i\}$ is a finite set of contractive similarities (called an *iterated function system*, IFS). Choose a bounded open set Ω whose closure contains K, and form the sequence of domains

$$\Omega_0 = \Omega, \quad \Omega_m = \bigcup F_i \Omega_{m-1} \text{ for } m \geq 1. \tag{1–2}$$

Consider the standard Laplacian Δ on Ω_m with Neumann boundary conditions (recall that such conditions make sense even for domains with rough boundary). Let $\{\lambda_n^{(m)}\}$ denote the eigenvalues in increasing order (repeated in case of nontrivial multiplicity) with eigenfunctions $\{u_n^{(m)}\}$ (L^2 normalized). So

$$-\Delta u_n^{(m)} = \lambda_n^{(m)} u_n^{(m)}. \tag{1–3}$$

Of course $\lambda_0^m = 0$ with u_0^m constant. We then hope to find a renormalization factor r such that

$$\lim_{m\to\infty} r^m \lambda_n^{(m)} = \lambda_n \tag{1–4}$$

exists and

$$\lim_{m\to\infty} u_n^{(m)}\big|_K = u_n \tag{1–5}$$

exists. (We have to be careful in cases of nontrivial multiplicity, and we may have to adjust $u_n^{(m)}$ by a minus sign in general.) If this is the case, then we may simply define a self-adjoint operator Δ on K by

$$-\Delta u_n = \lambda_n u_n. \tag{1–6}$$

Of course we would also like to identify Δ with a previously defined Laplacian, if such is possible, or at least show that Δ is a local operator satisfying some sort of self-similarity.

This may seem like wishful thinking, but it is not implausible. After all, many other types of structures on fractals can be obtained as limits of structures on Ω_m, so why not a Laplacian? After reading this paper, we hope the reader will agree that there is considerable evidence that this method should work in many cases. We leave to the future the challenge of describing exactly when it works, and why.

We note one great advantage of our method: it not only approximates the Laplacian, but it gives information about the spectrum. Other methods of constructing Laplacians on fractals do not yield spectral information directly. Of course, not all spectral information is immediately available. In particular, asymptotic information must be lost, since we know from Weyl's law that $\lambda_n^{(m)} = O(n)$ for each fixed m, but for fractals' Laplacians this is not the case. This means, in particular, that the limit (1–4) is not uniform in n. To get information about λ_n for large n requires taking a large value for m. In practice, our numerical calculations get stuck around $m = 4$. So we see only an approximation to a segment at the bottom of the spectrum. But this is already enough to reveal aspects of the spectrum that are provable. Briefly, if the fractal has a nontrivial finite group of symmetries, then every Neumann eigenfunction can be miniaturized, and so there is an eigenvalue renormalization factor R such that if λ is an eigenvalue then so is $R\lambda$. The argument for this works for the approximating domains and also for a self-similar Laplacian on the fractal. (In fact, the argument could be presented on the fractal alone, so its validity is independent of the validity of the outer approximation method, but in fact it was discovered by examining the experimental data!)

So what is the evidence for the validity of the outer approximation method? First we show that it works for the case that K is the unit interval (embedded in the x-axis in the plane). In this case we can take $F_0(x, y) = \left(\frac{1}{2}x, \frac{1}{2}y\right)$ and $F_1(x, y) = \left(\frac{1}{2}x + \frac{1}{2}, \frac{1}{2}y\right)$. If we take Ω to be the unit square, then we can compute the spectra of Ω_m (rectangles) and verify everything by hand ($r = 1$ in this case). We do this in Section 2, where we also look at different choices of Ω, producing sawtooth-shaped domains, whose spectra are computed numerically.

In Section 3 we look at the case of SG, where the spectrum is known exactly. Here we see numerically how the spectra of the approximating domains approach the known spectra. This computation shows that the accuracy falls off rapidly as n increases. We are also able to compare the eigenfunctions of the approximating domains with the known eigenfunctions on SG. In this case

it is natural to take Ω to be a triangle containing SG in its interior, since this yields connected domains Ω_m. We examine how the size of the overlap influences the spectra. After the work reported in Section 3 was completed, a different approach to outer approximation on SG was studied in [Blasiak et al. 08]. In particular, different methods for choosing approximating domains are used, and a whole family of different Laplacians is studied.

In Section 4 we examine numerical data for some fractals for which very little had been known about the spectrum of the Laplacian, and in some cases where even the existence of a Laplacian is unknown. These examples fall outside of the postcritically finite (PCF) category defined in [Kigami 01]. The first example is the standard Sierpiński carpet SC (cut out the middle square in tic-tac-toe and iterate). Here it is known that a self-similar Laplacian exists [Barlow 95], but the construction is indirect, and uniqueness is not known. (After this work was completed, uniqueness was established in [Barlow et al. 08].) But we also examine some nonsymmetric variants of SC for which the existence of a Laplacian is unknown. We also examine a symmetric fractal, the octagasket, where existence of a Laplacian is unknown. In all cases the spectra of the approximating regions appear to converge when appropriately renormalized. We can identify features of the spectrum, such as multiple eigenvalues and eigenvalue renormalization factors R, and we produce rough graphs of eigenfunctions on the fractal. In particular, there is no discernible difference between the behavior in the case of the standard SC and the other examples.

In Section 5 we describe the miniaturization process that produces the eigenvalue renormalization factor. For this to work we need a dihedral group of symmetries of the fractal. We deal only with the examples at hand, but it is clear that it works quite generally (we also explain how it works on the square). For the approximating regions, this shows how $R'\lambda_n^{(m)}$ shows up in the spectrum on Ω_{m+1} (the factor R' is not the same as R).

In Section 6 we examine numerical data of randomly constructed variants of SC, where the existence of Laplacians is unknown. To make these carpets, we modify the construction of SC. We fix the number of squares cut out at each recursive step, but we randomly determine which squares are removed. Then, we achieve connected domains Ω_m with a suitable change to the above algorithm and properly chosen parameters. Here we again see convergence of normalized eigenvalues. These random carpets are related to the Mandelbrot percolation process. See [Chayes et al. 88] and [Broman and Camia 08], for example.

How do we compute the spectrum of the Laplacian on the approximating domain? We use a finite-element-method solver, Matlab's `pdeeig` function. To do this we need only describe the geometry of the polygonal domain Ω_m. Then we either choose a triangulation (exclusive to Section 6) or let Matlab's triangulation functions `decsg` and `initmesh` produce a triangulation and then use piecewise linear splines in the finite-element method. Note that it would be preferable to use higher-order splines, at least piecewise cubic, since these increase accuracy dramatically for a fixed memory space and running time. As a concession, all of our triangulations may be further refined with the `refinemesh` function. The advantage of automating the triangulation is that it saves a tremendous amount of work; in particular, it chooses nonregular triangulations that increase accuracy. The disadvantage is that the program usually does not pick a triangulation with the same symmetry as the domain. This means that the eigenspaces that have nontrivial multiplicity in the domain end up being split into clusters of eigenspaces with eigenvalues close but not quite equal. Since much of the structure of the spectrum we are trying to observe has to do with multiplicities, this forces us to make ad hoc judgments as to when we have close but unequal eigenvalues versus multiple eigenvalues.

Why do we deal exclusively with Neumann spectra? The main reason is that Neumann boundary conditions on the approximating domains appear to lead to Neumann boundary conditions for the Laplacian on the fractal in the case of the interval and SG, while at the same time Dirichlet boundary conditions on the approximating domains do not lead to Dirichlet boundary conditions for the Laplacian on the fractal. For example, in the case of the interval you would need to use a mix of Dirichlet and Neumann boundary conditions on different portions of the boundary. It is not at all clear what to do for other fractals. Indeed, for SC it is not even clear what to choose for the boundary. The advantage of Neumann boundary conditions is that one can dispense with all notions of boundary, and define eigenfunctions simply as stationary points of the Rayleigh quotient with no boundary restrictions. All our programs, as well as further numerical data are available online.[1]

Finally, we note that [Kuchment and Zeng 01] considers similar outer approximations in the context of quantum graphs.

[1] At www.math.cornell.edu/~thb9d and www.math.cornell.edu/~smh82.

2. THE UNIT INTERVAL

For the unit interval I with the second derivative as Laplacian, the Neumann eigenfunctions are $\cos n\pi x$ with eigenvalues $(\pi n)^2$. If we take Ω to be the unit square, then Ω_m is the rectangle $[0,1] \times [0, 2^{-m}]$, with Neumann eigenfunctions $\cos n\pi x \cos 2^m k\pi y$ and eigenvalues $(\pi n)^2 + (\pi 2^m k)^2$. If we restrict attention to a fixed bottom segment of the spectrum, we will see eigenvalues with $k = 0$ just for m large enough (specifically, eigenvalues up to L, for $L \le (\pi 2^m)^2$). So $\lambda_n^{(m)} = \lambda_n$ exactly for large enough m. Of course, the corresponding eigenfunctions restricted to the interval give the exact eigenfunctions of the Laplacian on the interval. Note that for each m there are many other eigenfunctions on Ω_m (those with $k \neq 0$), but they are "blown away" in the limit. A similar analysis holds if we start with Ω equal to any rectangle with sides parallel to the axes. Note that we do not have to renormalize the spectrum, or equivalently, we can take $r = 1$ in (1–4).

We also note how other structures on I may be approximated from corresponding structures on Ω_m. For example, Lebesgue measure on I is the limit of Lebesgue measure on Ω_m suitably renormalized in the sense that

$$\lim_{m\to\infty} 2^m \iint_{\Omega_m} u(x,y)\,dx\,dy = \int_0^1 u(x,0)\,dx \qquad (2\text{–}1)$$

if $u(x,y)$ is continuous on Ω (the result is independent of the continuous extension $u(x,y)$ to Ω of $u(x,0)$ on I). A similar result holds for energy, provided we use the minimum energy extension. In other words, given $f \in H^1(I)$, let u be the minimum energy function with $u(x,0) = f(x)$. Then

$$\lim_{m\to\infty} 2^m \iint_{\Omega_m} |\nabla u(x,y)|^2\,dx\,dy = \int_0^1 |f'(x)|^2\,dx. \qquad (2\text{–}2)$$

In order to see this we expand f in a Fourier cosine series

$$f(x) = \sum_{k=0}^{\infty} a_k \cos \pi n x, \qquad (2\text{–}3)$$

for which we have

$$\int_0^1 |f'(x)|^2\,dx = \frac{1}{2}\sum_{k=1}^{\infty} (\pi k)^2 |a_k|^2. \qquad (2\text{–}4)$$

The minimum-energy extension to Ω_m is easily seen to be

$$u(x,y) = a_0 + \sum_{k=1}^{\infty} a_k \cos \pi k x \frac{\cosh 2\pi k(2^{-m} - y)}{\cosh \pi k 2^{-m}} \qquad (2\text{–}5)$$

with

$$\int_{\Omega_m} |\nabla u(x,y)|^2\,dx\,dy = \sum_{k=1}^{\infty} |a_k|^2 \pi k \left(\frac{\sinh 2\pi k 2^{-m}}{4\cosh^2 \pi k 2^{-m}}\right). \qquad (2\text{–}6)$$

Then (2–2) follows from (2–4) and (2–6). Note that we obtain the same result if we use the simpler extension $u(x,y) = f(x)$, although this extension does not minimize energy. (The energy-minimizing extension must be harmonic on the interior and satisfy Neumann boundary conditions on the portion of the boundary of Ω_m disjoint from I, and this explains (2–5).) We also have a bilinear version: Let

$$\mathcal{E}_I(f,g) = \int_0^1 f'(x)g'(x)\,dx \qquad (2\text{–}7)$$

and

$$\mathcal{E}_m(u,v) = \int_{\Omega_m} (\nabla u \cdot \nabla v)\,dx\,dy. \qquad (2\text{–}8)$$

If u_m and v_m denote the minimum-energy extensions of f and g to Ω_m, then

$$\lim_{m\to\infty} 2^m \mathcal{E}_m(u_m, v_m) = \mathcal{E}_I(f,g). \qquad (2\text{–}9)$$

We can use this to "define" a Laplacian on I via the weak formulation

$$\mathcal{E}_I(f,g) = -\int_0^1 f''(x)g(x)\,dx \qquad (2\text{–}10)$$

if g vanishes at 0 and 1. By the usual Gauss–Green formula,

$$\mathcal{E}_m(u_m, v_m) = \int_{\partial\Omega_m} (\partial_n u_m) v_m, \qquad (2\text{–}11)$$

and $\partial_n u_m = 0$ on all of $\partial\Omega_m$ except I, where $\partial_n u_m = -\frac{\partial}{\partial y} u_m$, so

$$\mathcal{E}_m(u_m, v_m) = -\int_0^1 \left(\frac{\partial u_m}{\partial y}\right) g\,dx. \qquad (2\text{–}12)$$

Combining (2–9), (2–10), and (2–12) yields, at least formally,

$$f''(x) = \lim_{m\to\infty} 2^m \frac{\partial u_m}{\partial y}(x,0). \qquad (2\text{–}13)$$

We can verify this by differentiating (2–5) directly (assuming that f is smooth enough) to obtain

$$\frac{\partial u_m}{\partial y}(x,0) = -\sum_{k=1}^{\infty} (\pi k)^2 a_k \cos \pi k x \left(\frac{\pi k \sinh 2\pi k 2^{-m}}{\cosh \pi k 2^{-m}}\right) \qquad (2\text{–}14)$$

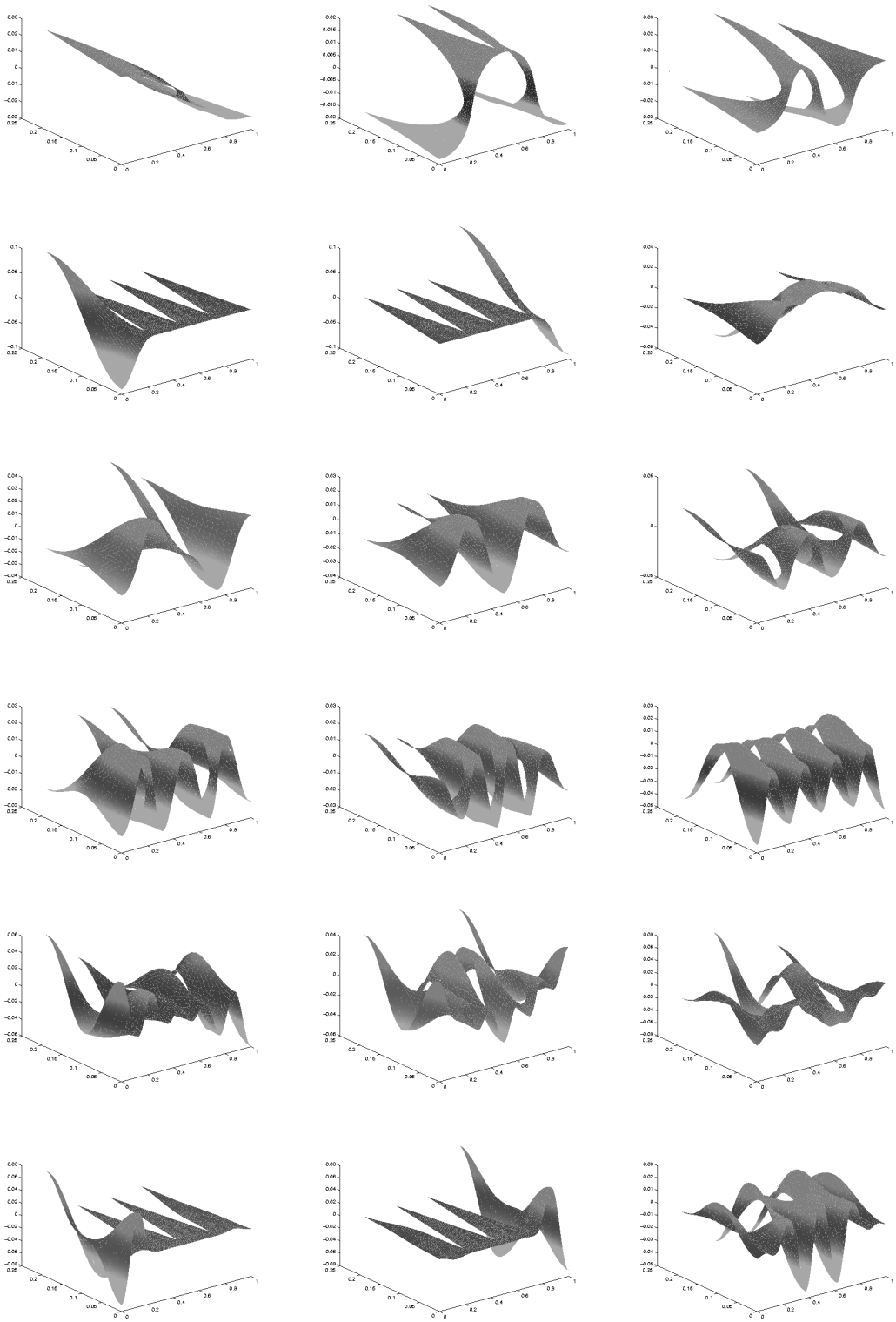

FIGURE 1. Sawtooth eigenfunctions, $m = 2$.

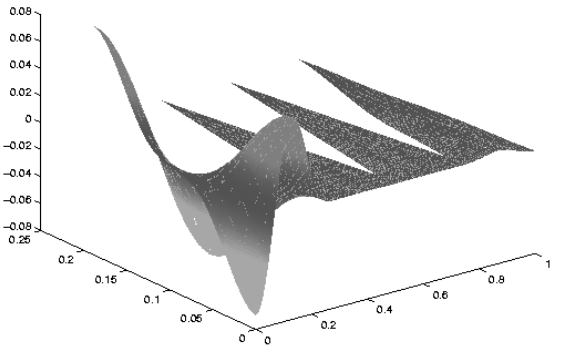

FIGURE 2. Almost localized sawtooth eigenfunction, $m = 2$.

and taking the limit to obtain

$$\lim_{m\to\infty} 2^m \frac{\partial u_m}{\partial y}(x,0) = -\sum_{k=1}^{\infty} (\pi k)^2 a_k \cos \pi k x, \qquad (2\text{–}15)$$

and this is the same value for $f''(x)$ that we obtain by differentiating (2–3) directly.

For a less-trivial example we need only take a geometrically more interesting Ω. In particular, let Ω be a triangle with vertices $(-\epsilon, 0)$, $(1+\epsilon, 0)$, and $\left(\frac{1}{2}, h\right)$ for some choice of positive parameters ϵ and h. Then Ω_m is a sawtooth region with 2^m teeth, maximum height $2^{-m}h$, and overlaps of length $2^{-m}\epsilon$. It is infeasible to compute the Neumann spectrum of the Ω_m exactly, so we use numerical methods. In Tables 1 and 3 we present the eigenvalues for several choices of parameters and level $m = 2, 3, 4$ (we also vary the number of refinements used in the FEM approximation). Actually, the computations are done for a similar image of Ω_m so that the base is exactly I, but this makes no difference in the limit. The evidence suggests that we get $c(\epsilon, h)\frac{d^2}{dx^2}$ in the limit for some constant that depends on the parameters.

In Tables 2 and 4 we present the same data, but we normalize by dividing $\lambda_n^{(m)}$ by $\lambda_1^{(m)}$. This enables us to compare the normalized eigenvalues with the expected values n^2. Note that with level $m = 5$ we see about a 1% deviation already at $n = 6$.

In Figure 1 we show some graphs of eigenfunctions on Ω_m that approximate eigenfunctions on I. In Figure 2 we show the graph of an eigenfunction on Ω_2 that does not approximate an eigenfunction on I. Indeed, this eigenfunction appears to be almost localized to one of the teeth. This phenomenon is discussed in [Heilman and Strichartz 10]. Unfortunately, we do not know whether we can define energy on I via (2–2) for a sawtooth region approximation. Indeed, we have no idea what the minimum-energy extension looks like.

There is yet another outer approximation approach to I, in which we regard it as the bottom line in SG. So we take $\Omega = \mathrm{SG}$ and $\Omega_{m+1} = F_1\Omega_m \bigcup F_2\Omega_m$. Then Ω_m is a fractafold in the sense of [Strichartz 03] consisting of 2^m cells of level m along the bottom of SG. The bottom 2^m Neumann eigenfunctions of the fractal Laplacian on Ω_m are obtained by the method of spectral decimation as follows. Fix a parameter j satisfying $0 \le j < 2^m$. Let $x_k = \frac{k}{2^m}$ for $0 \le k \le 2^m$ denote the points along I where the cells of Ω_m intersect, and let y_k for $1 \le k \le 2^m$ denote the top vertices of the cells (so cell number k has vertices x_{k-1}, x_k, y_k). Then u_j restricted to these points is defined by

$$\begin{aligned} u_j(x_k) &= \frac{1}{2}(\cos \pi j x_k + \cos \pi j x_{k+1}), \\ u_j(y_k) &= \cos \pi j x_k. \end{aligned} \qquad (2\text{–}16)$$

One can check that for a graph Laplacian Δ_m on the graph $\{x_k, y_k\}$ we have

$$-\Delta_m u_y = \left(2 - 2\cos\frac{\pi j}{2^m}\right) u_j \qquad (2\text{–}17)$$

with the appropriate Neumann conditions at the boundary points x_0, x_{2m}. Let

$$\phi_-(t) = \frac{5 - \sqrt{25 - 4t}}{2} \qquad (2\text{–}18)$$

and

$$\Phi(t) = \lim_{n\to\infty} 5^n \phi_-^{(n)}(t), \qquad (2\text{–}19)$$

where $\phi_-^{(n)}(t)$ denotes n-fold composition. In particular, Φ is a smooth function with $\Phi(0) = 0$ and $\Phi'(0) = 1$. Then the method of spectral decimation (see [Strichartz 06] for a detailed explanation) says that u_j may be extended to eigenfunctions of the fractal Laplacian on Ω_m with eigenvalue

$$\begin{aligned} \lambda_j^{(m)} &= \frac{3}{2} \lim_{n\to\infty} 5^{m+n} \phi_-^{(n)} \left(2 - 2\cos\frac{\pi j}{2^m}\right) \qquad (2\text{–}20) \\ &= \frac{3}{2} 5^m \Phi\left(2 - 2\cos\frac{\pi j}{2^m}\right). \end{aligned}$$

Now observe that $2 - 2\cos\frac{\pi j}{2^m} \approx (\frac{\pi j}{2^m})^2$ for large m, so

$$\lim_{m\to\infty} \left(\frac{4}{5}\right)^m \lambda_j^{(m)} = \frac{3}{2}(\pi j)^2. \qquad (2\text{–}21)$$

Of course, $(\pi j)^2$ is the correct eigenvalue for the eigenfunction $\cos \pi j x$ on I, which is clearly the limit of u_j as $u \to \infty$.

Level	2	2	2	2	3	3	3	3	4	4	4	4
Ref.	1	2	3	4	1	2	3	4	1	2	3	4
n												
1	4.905	4.823	4.790	4.777	4.868	4.789	4.756	4.743	4.828	4.749	4.717	4.703
2	17.980	17.662	17.535	17.483	19.097	18.782	18.655	18.602	19.218	18.903	18.776	18.724
3	33.418	32.790	32.53	32.436	41.513	40.808	40.525	40.408	42.900	42.191	41.906	41.787
4	246.809	243.909	243.176	242.991	69.950	68.724	68.232	68.029	75.398	74.140	73.635	73.425
5	246.809	243.910	243.176	242.991	100.984	99.165	98.436	98.134	116.012	114.066	113.283	112.958
6	248.850	246.991	246.524	246.407	129.818	127.424	126.463	126.064	163.836	161.053	159.935	159.471
7	250.833	248.743	248.218	248.087	150.737	147.863	146.713	146.238	217.674	213.915	212.408	211.783
8	253.564	251.508	250.992	250.863	959.592	952.139	950.177	949.677	276.002	271.161	269.220	268.417
9	337.235	332.179	330.654	330.157	959.592	952.139	950.177	949.677	336.966	330.967	328.563	327.569
10	389.324	382.371	380.228	379.513	970.250	963.501	961.797	961.369	398.337	391.162	388.285	387.094

TABLE 1. Sawtooth unnormalized eigenvalues, built with equilateral triangles. Equilateral triangles sawtooth region (height determined by requirement that triangles be equilateral; overlaps set to $(2^{-m})/10$) (Ref. = Refinement).

Level	2	2	2	2	3	3	3	3	4	4	4	4
Ref.	1	2	3	4	1	2	3	4	1	2	3	4
n												
1	1.000	1.000	1.000	1.000	1.000	1.000	1.000	1.000	1.000	1.000	1.000	1.000
2	3.665	3.662	3.661	3.660	3.923	3.922	3.922	3.922	3.981	3.981	3.981	3.981
3	6.813	6.798	6.793	6.790	8.527	8.522	8.520	8.519	8.886	8.885	8.884	8.884
4	50.316	50.570	50.764	50.870	14.368	14.352	14.345	14.343	15.618	15.613	15.612	15.611
5	50.316	50.570	50.764	50.870	20.742	20.709	20.695	20.690	24.030	24.021	24.017	24.016
6	50.732	51.209	51.463	51.585	26.665	26.610	26.588	26.578	33.936	33.916	33.908	33.905
7	51.136	51.572	51.816	51.936	30.962	30.878	30.845	30.832	45.088	45.048	45.033	45.027
8	51.693	52.145	52.395	52.518	197.104	198.834	199.766	200.222	57.170	57.104	57.078	57.068
9	68.750	68.871	69.025	69.118	197.104	198.834	199.766	200.222	69.797	69.698	69.659	69.644
10	79.370	79.277	79.374	79.450	199.293	201.207	202.209	202.687	82.510	82.375	82.321	82.299

TABLE 2. Sawtooth normalized eigenvalues, built with equilateral triangles. Equilateral triangles sawtooth region (height determined by requirement that triangles be equilateral; overlaps set to $(2^{-m})/10$) (Ref. = Refinement).

Level	2	2	2	2	3	3	3	3	4	4
Height	0.100	0.010	0.001	0.0005	0.100	0.010	0.001	0.0005	0.100	0.010
Ref.	2	2	2	2	2	2	2	2	2	2
n										
1	6.256	7.155	7.550	8.017	5.093	6.996	7.229	7.326	3.836	6.782
2	23.467	26.916	29.096	31.996	20.023	27.616	28.606	29.123	15.210	27.041
3	45.256	52.154	56.017	60.827	43.675	60.656	63.040	64.508	33.701	60.510
4	294.835	327.674	331.873	333.511	73.960	103.746	108.178	111.071	58.625	106.725
5	319.781	356.983	368.346	377.480	107.475	152.707	159.642	163.925	89.037	164.994
6	388.559	435.688	465.781	504.639	139.164	200.594	210.056	214.981	123.691	234.348
7	478.443	535.783	582.431	651.190	162.497	237.152	248.566	253.227	161.172	313.478
8	696.381	851.228	1007.893	1106.376	1017.767	1277.229	1293.087	1295.630	199.921	400.647
9	766.306	930.457	1254.199	1439.666	1027.972	1304.205	1326.104	1331.648	238.235	493.580
10	890.920	1092.418	1677.158		1068.070	1393.716	1422.250	1432.226	274.559	589.334

Level	4	4	5	5	5	4	4	4	4	5
Height	0.001	0.0005	0.100	0.010	0.001	0.100	0.010	0.001	0.0005	0.001
Ref.	2	2	2	2	2	3	3	3	3	3
n										
1	7.060	7.155	2.867	6.341	6.981	3.795	6.768	7.011	7.061	6.931
2	28.154	28.543	11.388	25.345	27.902	15.046	26.987	27.957	28.160	27.704
3	63.022	63.921	25.325	56.948	62.698	33.341	60.387	62.567	63.035	62.251
4	111.207	112.857	44.286	101.047	111.258	58.004	106.506	110.372	111.227	110.461
5	172.017	174.690	67.757	157.493	173.423	88.094	164.649	170.667	172.045	172.175
6	244.478	248.465	95.054	226.090	248.988	122.397	233.848	242.467	244.511	247.185
7	327.260	332.860	125.431	306.595	337.691	159.508	312.794	324.432	327.290	335.229
8	418.579	426.082	158.038	398.709	439.215	197.867	399.751	414.783	418.596	435.987
9	516.082	525.745	192.104	502.074	553.181	235.820	492.443	511.178	516.074	549.076
10	616.709	628.727	226.653	616.269	679.138	271.805	587.934	610.581	616.660	674.045

TABLE 3. Sawtooth unnormalized eigenvalues. Eigenvalue data for sawtooth regions with different parameters (Ref. = Refinement).

Level	2	2	2	2	3	3	3	3	4	4
Height	0.100	0.010	0.001	0.0005	0.100	0.010	0.001	0.0005	0.100	0.010
Refinement	2	2	2	2	2	2	2	2	2	2
n										
1	1.000	1.000	1.000	1.000	1.000	1.000	1.000	1.000	1.000	1.000
2	3.751	3.762	3.854	3.991	3.931	3.947	3.957	3.975	3.965	3.987
3	7.234	7.289	7.419	7.587	8.575	8.670	8.721	8.805	8.786	8.922
4	47.131	45.799	43.955	41.602	14.521	14.829	14.965	15.160	15.283	15.737
5	51.119	49.895	48.786	47.086	21.102	21.827	22.084	22.375	23.211	24.328
6	62.113	60.896	61.690	62.948	27.323	28.671	29.059	29.343	32.245	34.554
7	76.481	74.886	77.140	81.228	31.905	33.897	34.386	34.564	42.015	46.222
8	111.320	118.976	133.491	138.007	199.828	182.557	178.882	176.844	52.117	59.075
9	122.498	130.049	166.113	179.581	201.832	186.413	183.449	181.760	62.105	72.778
10	142.418	152.687	222.132		209.704	199.207	196.750	195.488	71.574	86.896

Level	4	4	5	5	5	4	4	4	4	5
Height	0.001	0.0005	0.100	0.010	0.001	0.100	0.010	0.001	0.0005	0.001
Refinement	2	2	2	2	2	3	3	3	3	3
n										
1	1.000	1.000	1.000	1.000	1.000	1.000	1.000	1.000	1.000	1.000
2	3.988	3.989	3.973	3.997	3.997	3.965	3.987	3.987	3.988	3.997
3	8.927	8.933	8.834	8.980	8.981	8.786	8.922	8.924	8.927	8.981
4	15.752	15.773	15.448	15.935	15.937	15.285	15.736	15.742	15.752	15.936
5	24.366	24.414	23.636	24.836	24.842	23.214	24.326	24.342	24.365	24.840
6	34.630	34.725	33.158	35.654	35.666	32.253	34.550	34.583	34.627	35.661
7	46.356	46.520	43.754	48.349	48.373	42.032	46.214	46.274	46.350	48.364
8	59.291	59.548	55.128	62.875	62.915	52.140	59.061	59.161	59.281	62.900
9	73.102	73.477	67.011	79.175	79.240	62.140	72.756	72.909	73.085	79.215
10	87.356	87.870	79.063	97.184	97.283	71.623	86.864	87.087	87.330	97.245

TABLE 4. Sawtooth normalized eigenvalues. Eigenvalue data for sawtooth regions with different parameters.

3. THE SIERPIŃSKI GASKET

Let $\{q_0, q_1, q_2\}$ denote the vertices of a unit-length equilateral triangle in the plane, and let $F_i x = \frac{1}{2}(x + q_i)$ for $i = 0, 1, 2$. Then SG is the invariant set for this IFS. We take Ω to be the equilateral triangle dilated by a factor $1 + \epsilon$. Then Ω_m is a union of 3^m triangles of size 2^{-m} that overlap in triangles of size $(1 + \epsilon)2^{-m}$.

In Tables 5 and 6 we present the same data as in Tables 1 through 4 for this example. The multiplicities and normalized eigenvalues agree with the known values for the Neumann spectrum of the standard Laplacian on SG [Strichartz 03]. For example, the first six distinct normalized eigenvalues on SG are 1, 5, 8.103, 10.305, 25, 31.784.

So the numerical accuracy improves as we decrease ϵ, but the error remains significant. (Much better accuracy is achieved in [Blasiak et al. 08].) Nevertheless, the qualitative features of the spectrum, including high multiplicities and large gaps, are already apparent. In Figure 3 we show some graphs of eigenfunctions. Actual graphs of Dirichlet eigenfunctions on SG may be found in [Dalrymple et al. 99].

In this case we know the eigenfunction renormalization factor $R = 5$, so we expect $r = 1.25$ in (1–4). The data are not inconsistent with this expectation, but it is impossible to deduce these values from the data alone.

We also look at the case $\epsilon = 0$, where the 3^m triangles in Ω_m intersect at single points. Thus the interior of Ω_m consists of 3^m disjoint triangles, and if we interpreted the Neumann Laplacian on Ω_m in the usual way, the spectrum would just be 3^m copies of the spectrum of Ω. This is nothing like the spectrum of SG, and also it is not what we get when we use the FEM. The reason is that the spline space chosen consists of continuous functions, and this effectively couples the disjoint triangles at their junction points.

Effectively this means that we are not looking at the entire Sobolev space $H^1(\Omega_m)$, but only the subspace $H_0^1(\Omega_m)$ defined to be the closure of continuous functions in $H^1(\Omega_m)$ in the Sobolev norm. In fact, functions in $H_0^1(\Omega_m)$ do not have to be continuous (or even bounded), since H^1 does not embed in continuous functions on $\mathbb{R}^2$. They do have to satisfy some integral continuity condition (see [Strichartz 67] for analogous results for $H^{1/2}$ on a half-line). The conclusion is that the Neumann

Sierpiński gasket eigenvalue data

Level	2	2	2	2	2	3	3	3	3	4	5
Ref.	0	1	2	3	4	0	1	2	3	0	0
n											
1	5.0727	4.8920	4.8223	4.7946	4.7832	4.1689	4.0255	3.9697	3.9473	3.3372	2.6327
2	5.0729	4.8924	4.8226	4.7948	4.7833	4.1690	4.0255	3.9697	3.9473	3.3376	2.6333
3	20.6394	19.9346	19.6622	19.5531	19.5080	18.2283	17.6218	17.3890	17.2965	15.0372	12.2130
4	20.6560	19.9498	19.6783	19.5698	19.5251	18.2452	17.6387	17.4059	17.3134	15.0492	12.2253
5	20.6657	19.9529	19.6796	19.5704	19.5254	18.2457	17.6389	17.4060	17.3135	15.0518	12.2256
6	35.4198	34.0098	33.4700	33.2558	33.1678	32.1806	31.0512	30.6141	30.4394	26.2223	20.8931
7	35.4331	34.0165	33.4733	33.2574	33.1685	32.1839	31.0522	30.6144	30.4394	26.2245	20.8956
8	43.3830	41.5793	40.8896	40.6160	40.5037	41.3292	39.8556	39.2856	39.0578	33.7524	26.8513
9	271.4544	266.9576	265.7778	265.4780	265.4017	83.0086	80.1965	79.1253	78.7016	71.6959	58.5692
10	271.5749	266.9740	265.7838	265.4848	265.4100	83.0336	80.2024	79.1260	78.7019	71.6980	58.5772

TABLE 5. SG unnormalized eigenvalues. (Ref. = Refinement).

	Sierpiński gasket eigenvalue data										
Level	2	2	2	2	2	3	3	3	3	4	5
Ref.	0	1	2	3	4	0	1	2	3	0	0
n											
1	1.0000	1.0000	1.0000	1.0000	1.0000	1.0000	1.0000	1.0000	1.0000	1.0000	1.0000
2	1.0000	1.0001	1.0001	1.0000	1.0000	1.0000	1.0000	1.0000	1.0000	1.0001	1.0002
3	4.0687	4.0750	4.0773	4.0781	4.0784	4.3724	4.3775	4.3805	4.3819	4.5059	4.6390
4	4.0720	4.0781	4.0807	4.0816	4.0820	4.3764	4.3817	4.3847	4.3862	4.5095	4.6437
5	4.0739	4.0787	4.0809	4.0818	4.0820	4.3766	4.3818	4.3847	4.3862	4.5103	4.6437
6	6.9824	6.9522	6.9407	6.9361	6.9342	7.7191	7.7136	7.7120	7.7115	7.8575	7.9360
7	6.9850	6.9535	6.9414	6.9364	6.9343	7.7199	7.7139	7.7121	7.7115	7.8582	7.9370
8	8.5522	8.4995	8.4793	8.4712	8.4678	9.9136	9.9008	9.8964	9.8949	10.1139	10.1992
9	53.5124	54.5705	55.1142	55.3701	55.4858	19.9112	19.9221	19.9324	19.9381	21.4837	22.2469
10	53.5361	54.5739	55.1155	55.3715	55.4876	19.9172	19.9236	19.9326	19.9382	21.4843	22.2499

	Spectral decimation eigenvalues	
Level	**Actual**	**Actual**
Ref.	**normalized**	**unnormalized**
n		
1	1.0000	27.1144
2	1.0000	27.1144
3	5.0000	135.5721
4	5.0000	135.5721
5	5.0000	135.5721
6	8.1039	219.7332
7	8.1039	219.7332
8	10.3056	279.4291
9	25.0000	677.8606
10	25.0000	677.8606

TABLE 6. SG normalized eigenvalues. (Ref. = Refinement).

Level	1	1	1	2	2	2	3	3	4	4
Ref.	2	3	4	2	3	4	3	4	3	4
n										
1	3.650	3.113	2.713	3.689	3.103	2.677	2.773	2.364	2.687	2.224
2	3.721	3.164	2.752	3.689	3.103	2.677	2.773	2.364	2.687	2.224
3	70.334	70.221	70.193	17.179	14.285	12.220	13.684	11.644	13.409	11.091
4	70.356	70.227	70.195	17.179	14.285	12.220	13.684	11.644	13.409	11.091
5	70.362	70.228	70.195	17.179	14.285	12.220	13.684	11.644	13.409	11.091
6	82.579	80.476	79.025	25.961	21.402	18.196	21.944	18.643	21.699	17.941
7	82.850	80.663	79.163	25.961	21.402	18.196	21.944	18.643	21.699	17.941
8	96.289	91.743	88.598	31.117	25.509	21.604	27.689	23.498	27.564	22.783
9	212.039	210.923	210.645	282.881	281.270	280.869	63.390	53.398	66.354	54.735
10	235.397	230.816	227.972	282.881	281.270	280.869	63.390	53.398	66.354	54.735

TABLE 7. Sierpiński gasket, no overlap, unnormalized. (Ref. = Refinement).

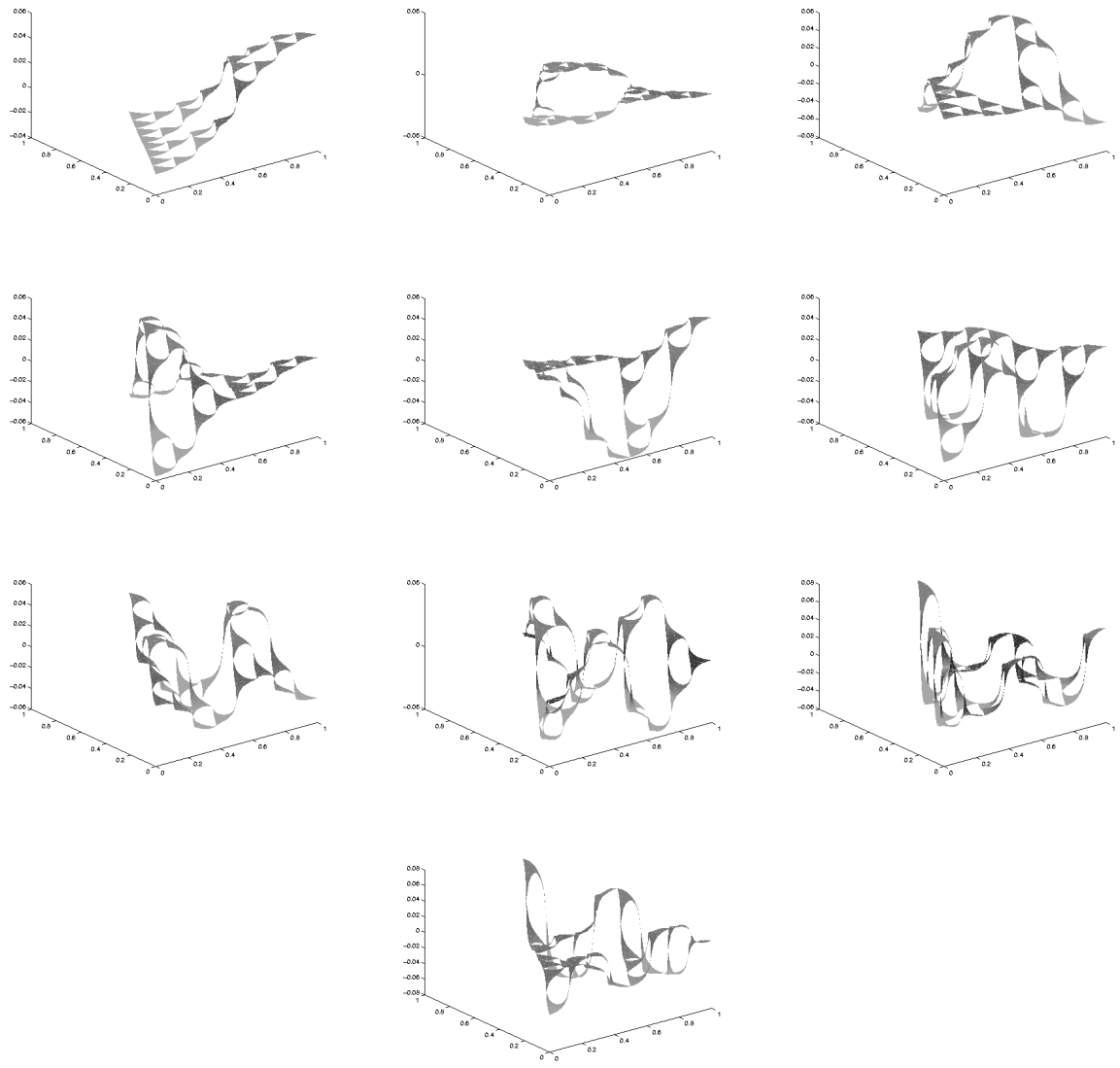

FIGURE 3. Sierpiński gasket (SG) eigenfunctions, level 3.

Level	1	1	1	2	2	2	3	3	4	4
Refinement	2	3	4	2	3	4	3	4	3	4
n										
1	1.000	1.000	1.000	1.000	1.000	1.000	1.000	1.000	1.000	1.000
2	1.019	1.016	1.014	1.000	1.000	1.000	1.000	1.000	1.000	1.000
3	19.268	22.557	25.875	4.657	4.604	4.564	4.935	4.925	4.990	4.987
4	19.274	22.559	25.876	4.657	4.604	4.564	4.935	4.925	4.990	4.987
5	19.275	22.559	25.876	4.657	4.604	4.564	4.935	4.925	4.990	4.987
6	22.622	25.851	29.131	7.037	6.897	6.796	7.914	7.886	8.075	8.067
7	22.697	25.911	29.182	7.037	6.897	6.796	7.914	7.886	8.075	8.067
8	26.378	29.470	32.660	8.435	8.221	8.069	9.986	9.939	10.257	10.244
9	58.087	67.754	77.650	76.680	90.646	104.909	22.861	22.586	24.692	24.612
10	64.486	74.144	84.038	76.680	90.646	104.909	22.861	22.586	24.692	24.612

TABLE 8. Sierpiński gasket, no overlap, normalized.

eigenvalues (and eigenfunctions) that the FEM approximates are the stationary values (and associated functions) for the Rayleigh quotient

$$R(u) = \frac{\int_{\Omega_m} |\nabla u|^2 \, dx}{\int_{\Omega_m} |u|^2 \, dx} \tag{3–1}$$

for some $u \in H_0^1(\Omega_m)$. Of course, some of these eigenfunctions restrict to Neumann eigenfunctions on each triangle in Ω_m and are continuous functions at the junction points, but it is easy to see that there are not enough of these (in fact, the smallest such eigenvalue must be of order of magnitude 4^m). We claim that all of the other eigenfunctions have poles at some junction points. Indeed, consider the restriction of an eigenfunction to a triangle. Because it is a Neumann eigenfunction, it must have vanishing normal derivatives along the side of the triangle. Choose a vertex of the triangle and reflect the eigenfunction evenly six times around.

This yields an eigenfunction in a deleted neighborhood of the vertex. The removable singularities theorem yields the following dichotomy: either the function is unbounded or it satisfies the eigenvalue equation at the vertex. If it satisfies the eigenvalue equation at all three vertices of the triangle, then the restriction to the triangle is a Neumann eigenvalue, contrary to our assumption. It is not difficult to see that the singularities must be logarithmic poles.

With this in mind, we look at the eigenvalue data in Tables 7 and 8. In contrast to our preceding computations, we do not see an apparent convergence of eigenvalues on a fixed Ω_m when we increase the refinement of the triangulation. In particular, the numerical values in Table 8 are even better than the data in Table 6. In other words, the poor approximations by the FEM to the actual eigenvalues on Ω_m yield very good approximations to the relative eigenvalues on SG. We can even extract rather decent estimates for $r = 1.25$ from the data in Table 7 if we pair off corresponding refinements at different levels. For example, if we compute $\lambda_n^{(3)}/\lambda_n^{(4)}$ using three refinements on level 3 and four refinements on level 4, then the first six distinct eigenvalues yield ratios 1.246, 1.233, 1.223, 1.158, 1.128, 1.112.

Of course, the eigenfunctions on Ω_m cannot approximate the eigenfunctions on SG, since the latter are bounded. Since we are already getting more information than we deserve, we might speculate that the eigenfunction approximation might be accurate in the complement of a small neighborhood of the junction points.

4. NON-PCF FRACTALS

Our first example is the octagasket, generated by eight contractive homotheties with contraction ratio $1 - \sqrt{2}/2$ and fixed points $\{q_i\}$ the vertices of a regular octagon. Then the consecutive images F_iK and $F_{i+1}K$ intersect along a Cantor set. As yet, there has been no construction of a self-similar Laplacian on this fractal, although it is reasonable to expect that the probabilistic methods in [Barlow 95] will work, given the high symmetry in this example.

It is natural to approximate from without by taking Ω to be the interior of the octagon with vertices $\{q_i\}$. Then Ω_m consists of the interior of the union of 8^m octagons that meet along edges.

In Table 9 we give the eigenvalues on Ω_m for $m = 0, 1, 2, 3$ along with level-to-level ratios, suggesting a renormalization factor of about $r = 1.2$. In Table 10 we normalize the eigenvalues by dividing by $\lambda_1^{(m)}$. This suggests an eigenvalue renormalization factor of about $R = 14.9476$ (the table indicates when a new eigenvalue appears that is approximately $R\lambda_n$ for an earlier value of n). In the next section we will explain why this happens. The tables show eigenvalues of multiplicities 1 and 2, but no higher multiplicities. The D_8 symmetry forces multiplicity 2, since there are three irreducible representations of dimension 2.

There are a number of close coincidences (for example 910.5058 and 910.8645, each with multiplicity 2), but not close enough to be regarded as the same, in our judgement. There is some evidence of large gaps in the spectrum, for example $(66.45202, 122.0411)$, $(162.1709, 223.2267)$, and $(253.6123, 336.1848)$. However, there is not enough data to guess whether there are infinitely many gaps ($\lambda_{j+1}/\lambda_j \geq 1 + \epsilon$ for fixed ϵ). In Figure 4 we display the graphs of some eigenfunctions, and in Figure 6 we show the Weyl ratios.

The Weyl ratio is defined to be $W(x) = N(x)/x^\alpha$, where $N(x) = \#\{\lambda_j \leq x\}$ is the eigenvalue-counting function, and x^α is its approximate growth rate. We determine α experimentally as the slope of the line of best fit to a log-log plot of $N(x)$.

The Weyl ratio gives a nice "snapshot" of the spectrum. A question of interest is whether it tends to a limit for large x or exhibits periodic behavior. Our experimental data do not give an indication of what answer to expect.

The next example we consider is the standard SC generated by eight contractions of ratio $\frac{1}{3}$ (omitting the

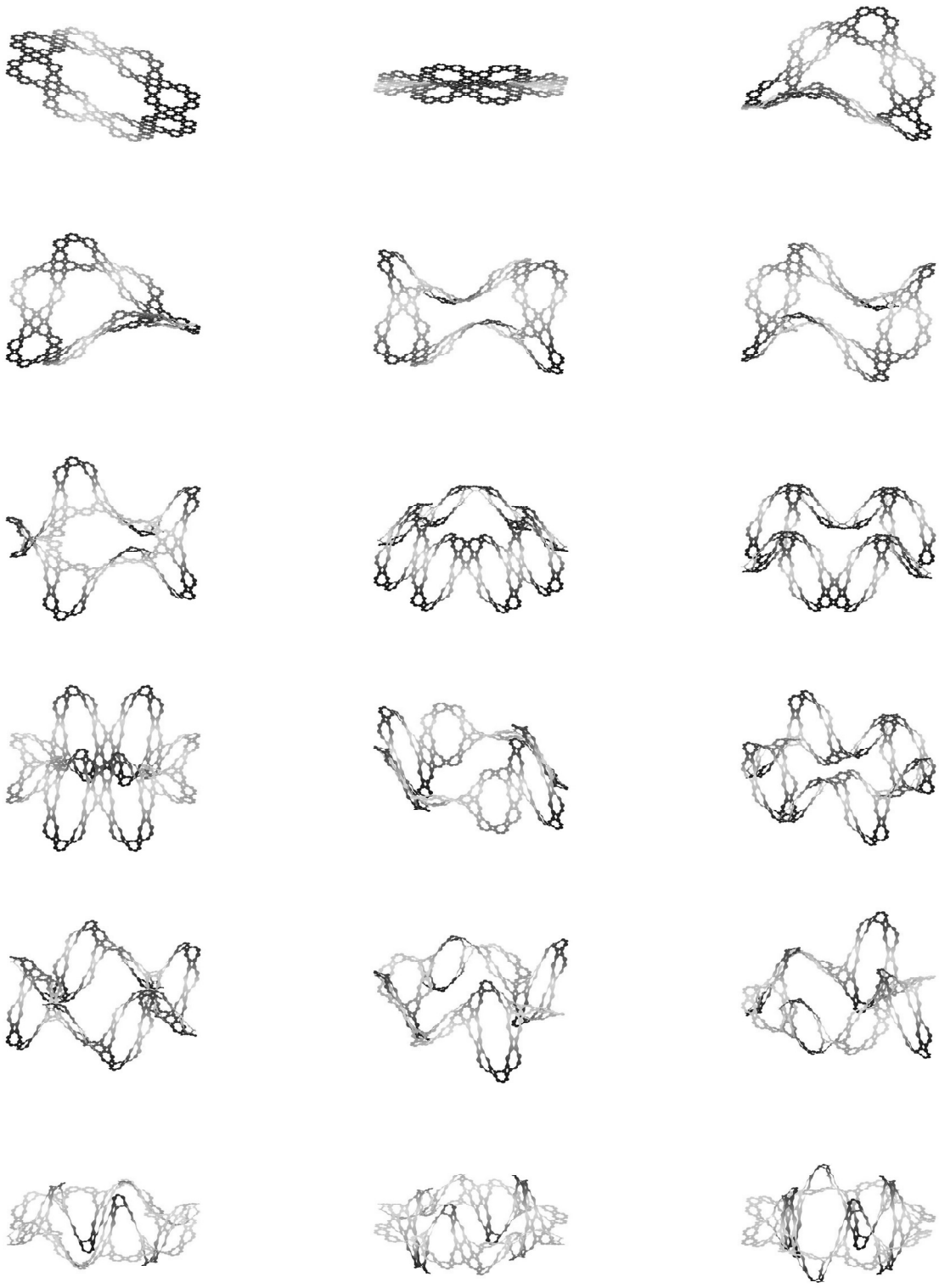

FIGURE 4. Octagasket eigenfunctions, level 3.

Level	1	1	2	2	2	2	3	3	3	3	4
Ref.	0	1	1	2	3	4	1	2	3	4	1
n											
1	12.87	12.81	6.28	6.14	6.08	6.06	5.07	4.86	4.78	4.74	3.95
2	12.87	12.81	6.30	6.15	6.09	6.06	5.07	4.86	4.78	4.74	3.95
3	35.55	35.14	23.98	23.37	23.14	23.04	19.15	18.37	18.04	17.90	14.93
4	35.56	35.15	24.00	23.38	23.14	23.04	19.15	18.37	18.04	17.90	14.93
5	57.06	55.93	47.97	46.60	46.08	45.88	38.75	37.15	36.47	36.20	30.19
6	67.47	66.00	48.24	46.70	46.12	45.90	38.75	37.15	36.47	36.20	30.19
7	67.49	66.00	62.46	60.28	59.47	59.17	53.10	50.89	49.96	49.58	41.32
8	99.03	95.78	151.54	149.80	149.30	149.17	75.96	72.75	71.40	70.86	59.09
9	112.63	108.51	151.61	149.81	149.31	149.17	75.96	72.75	71.40	70.86	59.09
10	112.78	108.55	154.94	152.84	152.22	152.04	78.99	75.65	74.25	73.68	61.42

j	1	2	3
n			
1	2.11	1.28	1.20
2	2.11	1.28	1.20
3	1.53	1.29	1.20
4	1.53	1.29	1.20
5	1.22	1.27	1.20
6	1.44	1.27	1.20
7	1.12	1.19	1.20
8	0.64	2.11	1.20
9	0.73	2.11	1.20
10	0.71	2.06	1.20

TABLE 9. Octagasket unnormalized eigenvalues (above) and ratios $\lambda_n^{(j)}/\lambda_n^{(j+1)}$ (below), highest refinements used.

Level	1	1	2	2	2	2	3	3	3	3	4
Ref.	0	1	1	2	3	4	1	2	3	4	1
n											
1	1.00	1.00	1.00	1.00	1.00	1.00	1.00	1.00	1.00	**1.00**	1.00
2	1.00	1.00	1.00	1.00	1.00	1.00	1.00	1.00	1.00	**1.00**	1.00
3	2.76	2.74	3.82	3.81	3.80	3.80	3.78	3.78	3.78	**3.78**	3.78
4	2.76	2.74	3.82	3.81	3.80	3.80	3.78	3.78	3.78	**3.78**	3.78
5	4.43	4.37	7.64	7.59	7.57	7.57	7.64	7.64	7.64	**7.64**	7.64
6	5.24	5.15	7.68	7.60	7.58	7.57	7.64	7.64	7.64	**7.64**	7.64
7	5.25	5.15	9.95	9.82	9.77	9.76	10.48	10.46	10.46	10.46	10.45
8	7.70	7.48	24.13	24.39	24.54	24.61	14.99	14.96	14.95	14.95	**14.95**
9	8.75	8.47	24.14	24.39	24.54	24.61	14.99	14.96	14.95	14.95	**14.95**
24	26.15	23.78	68.29	67.39	67.30	67.36	57.38	56.96	56.84	56.81	**56.47**
25	28.02	25.18	68.68	67.47	67.32	67.37	57.38	56.96	56.84	56.81	**56.47**
40	51.26	43.52	119.34	114.57	113.44	113.23	116.01	113.96	113.36	113.17	**114.27**
41	51.72	43.63	120.99	115.04	113.54	113.26	116.01	113.96	113.36	113.17	**114.27**

TABLE 10. Octagasket normalized eigenvalues. Eigenvalues in boldface on level 4 are approximately R (where R =14.95) times the eigenvalues in boldface on level 3. (Ref. = Refinement).

middle tic-tac-toe square). Here the existence of a self-similar Laplacian is known, and as stated above, uniqueness is established in [Barlow et al. 08]. Here it is natural to choose Ω to be the interior of the square that contains just SC, so Ω_m contains 8^m squares of side length 3^{-m} intersecting along edges. In Tables 11 and 12 we report unnormalized and normalized eigenvalue data, as before. In Table 13 we describe the D_4 representation type associated with the eigenspace. There is one 2-dimensional representation (denoted by 2) and four 1-dimensional representations ($1++$, $1+-$, $1-+$, and $1--$) described in more detail in the next section. Again we see eigenvalue multiplicities of only 1 or 2. There is an apparent eigenvalue renormalization factor of about $R = 10.0081$, which is consistent with computations in [Barlow et al. 90]. In the next section we will give an explanation of this behavior. Spectral gaps are consistent with the data. Figure 5 shows some eigenfunctions, and Figure 7 shows the Weyl ratios.

The last two examples we consider are alternative carpets. We subdivide the unit square into 16 subsquares of side length $\frac{1}{4}$, and retain all but the four inner squares ($\frac{12}{16}$ carpet) or all but three of the inner squares ($\frac{13}{16}$ carpet). The $\frac{12}{16}$ carpet has D_4 symmetry, and it is known

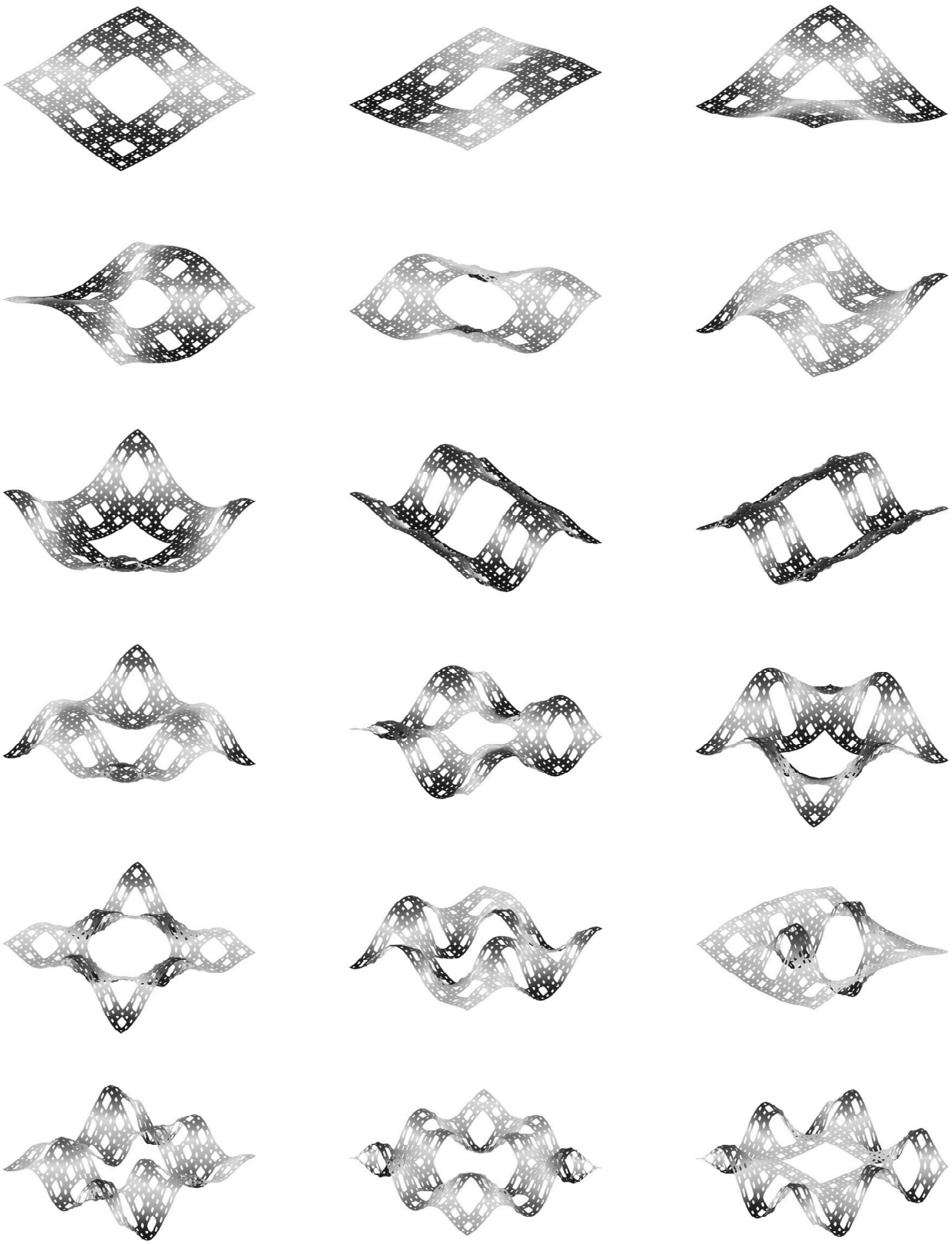

FIGURE 5. Sierpiński carpet (SC) eigenfunctions, level 4.

Level	1	1	1	1	1	2	2	2	2	3	3	3	3
Ref.	0	1	2	3	4	0	1	2	3	0	1	2	3
n													
1	6.9095	6.8043	6.7653	6.7505	6.7449	6.4313	6.2251	6.1354	6.10	5.87	5.6310	5.5325	5.4936
2	6.9151	6.8070	6.7664	6.7510	6.7451	6.4323	6.2254	6.1355	6.10	5.87	5.6310	5.5325	5.4936
3	18.9925	18.8600	18.8243	18.8150	18.8127	17.0488	16.5574	16.3441	16.26	15.57	14.9425	14.6841	14.5823
4	34.3954	33.3153	32.9506	32.8218	32.7746	32.1097	30.7611	30.2096	30.00	28.99	27.7633	27.2621	27.0651
5	47.0332	45.9328	45.6120	45.5142	45.4829	42.8446	41.1639	40.4941	40.24	38.71	37.0938	36.4341	36.1754
6	47.1243	45.9546	45.6175	45.5157	45.4834	42.8729	41.1729	40.4965	40.24	38.71	37.0938	36.4341	36.1754
7	52.1193	51.1387	50.8862	50.8221	50.8059	44.8902	43.1147	42.3923	42.12	40.48	38.7875	38.0972	37.8262
8	92.8584	89.8444	89.0822	88.8905	88.8425	66.1417	62.7984	61.4619	60.97	58.99	56.4159	55.3699	54.9598
9	93.0125	89.8865	89.0933	88.8933	88.8432	66.2982	62.8473	61.4753	60.97	58.99	56.4159	55.3699	54.9598
10	99.0749	95.5391	94.6410	94.4145	94.3576	71.9960	68.3327	66.9090	66.39	64.16	61.3551	60.2173	59.7724

TABLE 11. SC unnormalized eigenvalues. (Ref. = Refinement).

Level	1	1	1	1	1	2	2	2	2	3	3	3	3
Ref.	0	1	2	3	4	0	1	2	3	0	1	2	3
n													
1	1.0000	1.0000	1.0000	1.0000	1.0000	1.0000	1.0000	1.0000	1.0000	1.0000	1.0000	1.0000	1.0000
2	1.0008	1.0004	1.0002	1.0001	1.0000	1.0002	1.0001	1.0000	1.0000	1.0000	1.0000	1.0000	1.0000
3	2.7488	2.7718	2.7825	2.7872	2.7892	2.6509	2.6598	2.6639	2.6657	2.6530	2.6536	2.6541	2.6544
4	4.9780	4.8962	4.8706	4.8621	4.8592	4.9927	4.9414	4.9238	4.9181	4.9383	4.9305	4.9276	4.9267
5	6.8070	6.7505	6.7421	6.7423	6.7433	6.6619	6.6126	6.6001	6.5973	6.5950	6.5875	6.5855	6.5850
6	6.8202	6.7537	6.7429	6.7425	6.7434	6.6663	6.6140	6.6005	6.5974	6.5950	6.5875	6.5855	6.5850
7	7.5431	7.5156	7.5217	7.5286	7.5325	6.9800	6.9259	6.9095	6.9052	6.8963	6.8882	6.8861	6.8855
8	13.4392	13.2040	13.1676	13.1679	13.1719	10.2844	10.0879	10.0176	9.9946	10.0497	10.0189	10.0081	10.0043
9	13.4615	13.2102	13.1692	13.1684	13.1720	10.3087	10.0958	10.0198	9.9951	10.0497	10.0189	10.0081	10.0043
10	14.3389	14.0409	13.9892	13.9862	13.9895	11.1947	10.9769	10.9055	10.8833	10.9307	10.8960	10.8843	10.8804

TABLE 12. SC normalized eigenvalues. (Ref. = Refinement).

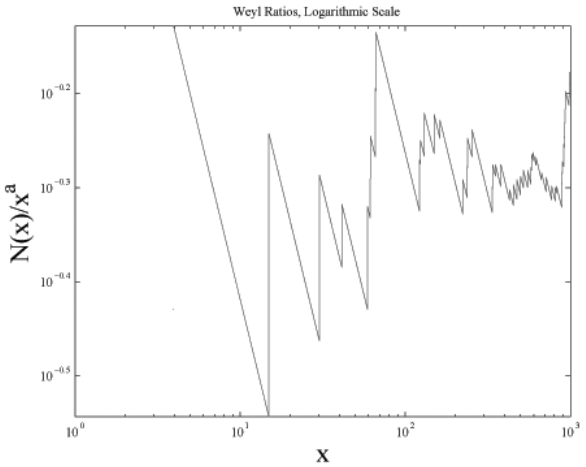

FIGURE 6. Octagasket Weyl ratios, level 4, one refinement, $\alpha = 0.71938$.

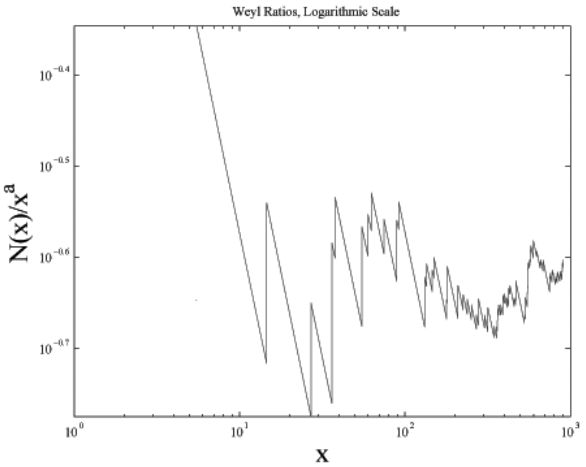

FIGURE 7. SC Weyl ratios, level 3, three refinements, $\alpha = 0.87392$.

that a self-similar Laplacian exists. The $\frac{13}{16}$ carpet has no symmetry, and the methods used to construct a Laplacian on SC do not work on this example. So the situation is even worse than for the octagasket.

In Tables 14 and 15 we present unnormalized and normalized eigenvalues for the $\frac{12}{16}$ carpet, and in Tables 16 and 17 the same data for the $\frac{13}{16}$ carpet. (Again we use the interior of the square for Ω.) In Figure 8 we show the Weyl ratios for the $\frac{12}{16}$ carpet, and in Figure 9 we show those for the $\frac{13}{16}$ carpet. The evidence for convergence is strong in both cases. But the nature of the spectrum is quite different. In the symmetric $\frac{12}{16}$ carpet, we see multiplicities of 1 or 2, and an eigenvalue renormalization factor of about $R = 20.123$. For the $\frac{13}{16}$ carpet we do not see any multiplicities above 1, and there is no apparent eigenvalue renormalization factor. The evidence for

Number	Eigenvalue	Type	Number	Eigenvalue	Type
1	5.4936	2	48	458.2523	1+ -
2	5.4936	2	49	467.2072	1- +
3	14.5823	1 + −	50	467.5056	2
4	27.0651	1 − +	51	467.5056	2
5	36.1754	2	52	528.0563	1- +
6	36.1754	2	53	533.2348	1+ +
7	37.8262	1 + +	54	535.0612	2
8	54.9598	2	55	535.0612	2
9	54.9598	2	56	549.3760	2
10	59.7724	1 + −	57	549.3760	2

TABLE 13. D_4 representation type. Sierpiński carpet, level 3, three refinements.

Level	1	1	1	2	2	2	3
Refinement	0	1	2	0	1	2	0
n							
1	5.184	5.108	5.079	4.246	4.119	4.065	3.38
2	5.194	5.113	5.081	4.246	4.119	4.065	3.38
3	16.788	16.699	16.673	13.176	12.805	12.649	10.47
4	25.029	24.128	23.805	20.638	19.903	19.593	16.37
5	43.231	42.181	41.846	33.584	32.459	31.992	26.58
6	43.301	42.210	41.858	33.584	32.459	31.992	26.58
7	58.008	56.942	56.648	42.636	41.255	40.689	33.70
8	93.773	89.292	87.948	70.623	68.005	66.881	55.56
9	101.704	98.004	96.965	70.623	68.005	66.961	55.56
10	102.074	98.095	96.985	70.890	68.023	66.961	55.62

TABLE 14. 12/16 symmetric carpet unnormalized eigenvalues.

Level	1	1	1	2	2	2	3
Refinement	0	1	2	0	1	2	0
n							
1	1.000	1.000	1.000	1.000	1.000	1.000	1.000
2	1.002	1.001	1.000	1.000	1.000	1.000	1.000
3	3.239	3.269	3.283	3.103	3.109	3.112	3.097
4	4.829	4.724	4.687	4.861	4.831	4.820	4.841
5	8.340	8.258	8.239	7.910	7.879	7.870	7.859
6	8.354	8.263	8.242	7.910	7.879	7.870	7.859
7	11.191	11.147	11.154	10.042	10.015	10.009	9.967
8	18.091	17.481	17.317	16.633	16.508	16.453	16.431
9	19.621	19.186	19.092	16.633	16.508	16.472	16.431
10	19.692	19.204	19.096	16.696	16.513	16.472	16.449

TABLE 15. 12/16 symmetric carpet normalized eigenvalues.

spectral gaps is also weaker for the $\frac{13}{16}$ carpet, but this is not conclusive.

5. MINIATURIZATION

In order to make the ideas clear, we begin by explaining the method of miniaturization on the unit interval I. Here we have a two-element group of symmetries consisting of the identity and the reflection $\rho(x) = 1 - x$ about the midpoint. Every Neumann eigenfunction is of the form $\cos \pi kx$. When k is even, the function is even under ρ, namely $u \circ \rho = u$, while if k is odd, then the function is odd, namely $u \circ \rho = -u$. In this way all eigenspaces are sorted corresponding to the two irreducible representations of the symmetry group. For every even eigenfunction u (except the constant), we can miniaturize it by defining u_+ to be

$$u_+(x) = \begin{cases} u \circ F_0^{-1} & \text{on } F_0 I, \\ u \circ F_1^{-1} & \text{on } F_1 I. \end{cases} \tag{5–1}$$

Note that $u \circ F_0^{-1}(\frac{1}{2}) = u \circ F_1^{-1}(\frac{1}{2})$ because u is even, and the derivative vanishes at $\frac{1}{2}$ because u is a Neumann eigenfunction, which shows that u_+ is also a Neumann eigenfunction, and indeed $u_+(x) = \cos 2\pi kx$. On the other hand, if u is an odd eigenfunction, then define u_-

Level	1	1	1	2	2	2	3
Refinement	0	1	2	0	1	2	0
n							
1	8.141	8.025	7.981	7.777	7.590	7.512	7.261
2	8.328	8.201	8.151	7.920	7.724	7.643	7.375
3	18.904	18.728	18.674	18.046	17.656	17.498	16.889
4	36.040	35.189	34.898	33.783	32.859	32.488	31.352
5	41.026	40.392	40.209	38.618	37.681	37.307	36.009
6	47.908	46.956	46.686	45.136	44.028	43.592	42.108
7	51.147	50.262	50.022	47.827	46.543	46.037	44.385
8	78.834	76.085	75.308	72.746	70.651	69.849	67.394
9	83.837	79.862	78.600	77.387	74.736	73.703	71.197
10	98.313	95.303	94.500	91.043	88.502	87.534	84.498

TABLE 16. 13/16 alternative carpet unnormalized eigenvalues.

Level	1	1	1	2	2	2	3
Refinement	0	1	2	0	1	2	0
n							
1	1.000	1.000	1.000	1.000	1.000	1.000	1.000
2	1.023	1.022	1.021	1.018	1.018	1.017	1.016
3	2.322	2.334	2.340	2.320	2.326	2.329	2.326
4	4.427	4.385	4.373	4.344	4.329	4.325	4.318
5	5.040	5.033	5.038	4.966	4.965	4.966	4.960
6	5.885	5.851	5.850	5.804	5.801	5.803	5.799
7	6.283	6.263	6.268	6.150	6.132	6.128	6.113
8	9.684	9.481	9.436	9.354	9.309	9.298	9.282
9	10.299	9.952	9.849	9.951	9.847	9.811	9.806
10	12.077	11.876	11.841	11.706	11.661	11.652	11.638

TABLE 17. 13/16 alternative carpet normalized eigenvalues.

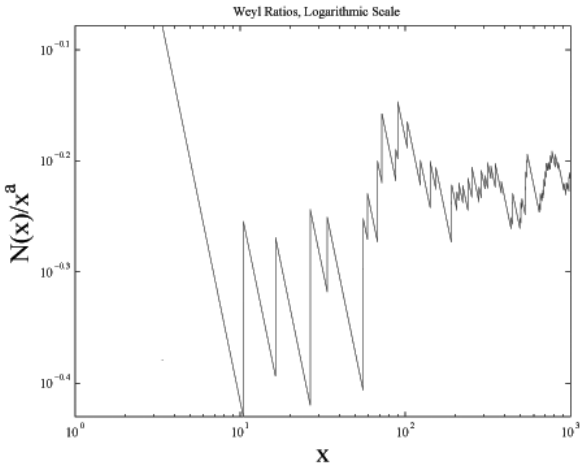

FIGURE 8. 12/16 carpet Weyl ratios, level 3, zero refinements, $\alpha = 0.71738$.

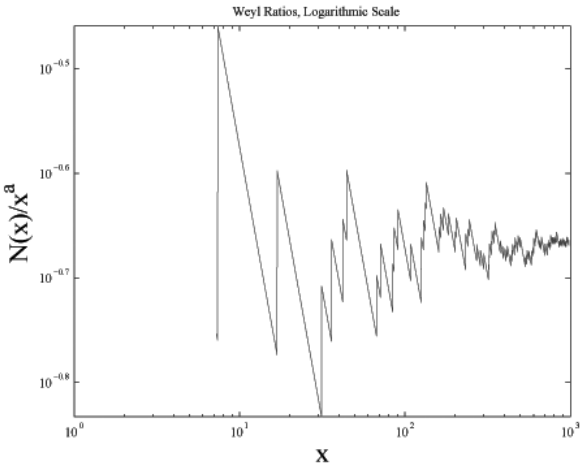

FIGURE 9. 13/16 carpet Weyl ratios, level 3, zero refinements, $\alpha = 0.87537$.

by

$$u_+(x) = \begin{cases} u \circ F_0^{-1} & \text{on } F_0 I, \\ -u \circ F_1^{-1} & \text{on } F_1 I. \end{cases} \tag{5–2}$$

Again $u \circ F_0^{-1}(\frac{1}{2}) = -u \circ F_1^{-1}(\frac{1}{2})$ because u is odd, so u_- is also a Neumann eigenfunction, and again $u_-(x) = \cos 2\pi kx$. We call u_+ or u_- the miniaturization of u. Note that the representation type of the miniaturization is always even. The eigenvalue of u_+ or u_- is always four times the eigenvalue of u. Thus $R = 4$ is an eigenvalue renormalization factor. (Of course I has other eigenvalue renormalization factors, namely any square integer, but such luxuries do not generalize to other fractals).

Now consider a self-similar fractal with a finite group of symmetries G, and suppose the Laplacian is

G-invariant. Then each eigenspace splits according to the irreducible representations of G. We seek to find a set of recipes, analogous to (5–1) and (5–2), to miniaturize eigenfunctions according to the corresponding irreducible representations of G. In fact, our goal is to obtain recipes that make sense on the fractal and also on the outer approximating domains. In the latter case, the miniaturization of an eigenfunction on Ω_m will be an eigenfunction on Ω_{m+1}.

It is by no means clear that this goal is always attainable. We will show explicitly that it is possible for SC, the $\frac{12}{16}$ carpet, and the octagasket. In the first two examples the symmetry group is D_4 (the dihedral symmetry group of the square), and in the last example it is D_8. In contrast to the interval, the representation type of the miniaturized eigenfunctions is the same as the original one.

The referee has pointed out that it is also possible to explain miniaturization on carpets using local reflection maps introduced in [Barlow and Bass 89] and [Barlow and Bass 99] (see also [Barlow et al. 08, Definition 2.12]).

We mention in passing that a version of miniaturization is valid for SG, but the recipes are more complicated. In particular, the multiplicities increase. This is part of the story of spectral decimation (see [Strichartz 06] for a description). On the other hand, it is not clear how to extend the recipes for the approximating domains Ω_m with a positive ϵ overlap, although they are presumably valid in the zero-overlap case.

The symmetry group D_4 has five irreducible representations. Let ρ_{H} and ρ_{V} denote the reflections about the horizontal and vertical axes in D_4, and let ρ'_{D} and ρ''_{D} denote the two diagonal reflections. The four one-dimensional representations $1++$, $1+-$, $1-+$, and $1--$ are characterized by parity with respect to these reflections. (Strictly speaking, we describe functions that transform according to the representations, rather than the abstract representations, since we are interested in eigenfunctions that transform according to representations.) Functions transforming according to $1++$ are even with respect to all reflections, and those transforming according to $1--$ are odd with respect to all reflections. The $1+-$ functions are odd with respect to ρ_{H} and ρ_{V} and even with respect to ρ'_{D} and ρ''_{D}, while for $1-+$ the reverse holds.

Now suppose u is a Neumann eigenfunction on Ω_m of $1++$ or $1-+$ type. Define the miniaturization

$$u_+ = \{u \circ F_i^{-1} \text{ on } F_i\Omega_m\} \text{ on } \Omega_{m+1} \tag{5–3}$$

for either the SC or $\frac{12}{16}$ carpet. On the other hand, for an eigenfunction of $1+-$ or $1--$ type define

$$u_- = \{\pm u \circ F_i^{-1} \text{ on } F_i\Omega_m\} \text{ on } \Omega_{m+1}, \tag{5–4}$$

where we alternate the choice of $\pm$ on neighboring cells (see Figure 10). Because of the even or odd parity of u with respect to the reflections ρ_{H} and ρ_{V}, the miniaturized functions are continuous along the boundaries of the cells of order one. Since u satisfies Neumann boundary conditions, it follows that u_+ or u_- satisfies matching conditions along these boundaries; hence they are Neumann eigenfunctions on u_{m+1}, and the eigenvalue is multiplied by λ^{-2}, where λ denotes the contraction ratio of the F_i mappings (so $\lambda = \frac{1}{3}$ for SC and $\lambda = \frac{1}{4}$ for the $\frac{12}{16}$ carpet). Note that on the $\frac{12}{16}$ carpet, the miniaturized eigenfunction has the same representation type as u, while on SC, u_+ preserves representation type while u_- maps $1+-$ to $1++$ and $1--$ to $1-+$.

There is also a two-dimensional representation of D_4, which we denote by 2. The representation space is spanned by functions u and v satisfying

$$v = \rho_{\mathrm{H}} u = -\rho_{\mathrm{V}} u$$

and

$$\rho''_{\mathrm{D}} u = -\rho'_{\mathrm{D}} u = u, \quad \rho'_{\mathrm{D}} v = -\rho''_{\mathrm{D}} v = v.$$

The miniaturized functions u_2 and v_2 are shown in Figure 11. Once again we see that u_2 and v_2 are Neumann eigenfunctions on Ω_{m+1} with eigenvalue multiplied by λ^{-2}, and the pair transform according to the representation 2.

What does this tell us about the Neumann spectrum on the corresponding fractal? If we believe (1–4), then there will be an eigenvalue renormalization factor $R = r\lambda^{-2}$. For every eigenvalue λ_n, there will be an eigenvalue equal to $R\lambda_n$ with equal multiplicity, and the corresponding eigenfunctions will be miniaturizations as illustrated.

But in fact, we can run the same miniaturization argument directly on the fractal. Indeed, in both cases we know that there exists a Laplacian Δ on the fractal satisfying a self-similar identity

$$\Delta(u \circ F_i) = R^{-1}(\Delta u) \circ F_i \tag{5–5}$$

for a certain constant R. Then the miniaturization recipes given above create eigenfunctions with eigenvalue multiplied by R. This is true independently of the validity of the outer approximation method. Incidentally, the miniaturization recipes given above extend easily to any D_4-symmetric-carpet-type fractal.

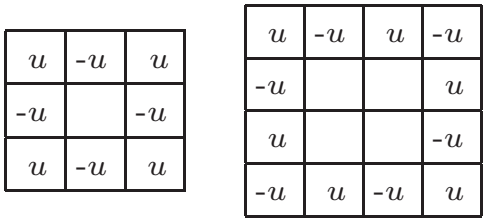

(a) (b)

FIGURE 10. One-dimensional miniaturized carpet eigenfunctions.

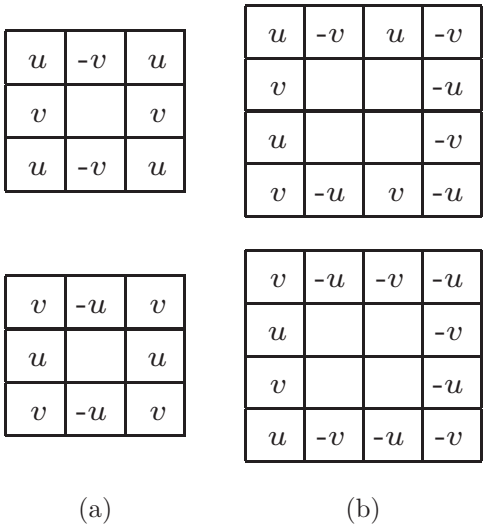

(a) (b)

FIGURE 11. One-dimensional miniaturized carpet eigenfunctions.

In our last example, the octagasket, the symmetry group is D_8. Here we have four one-dimensional representations. Since $D_4 \subset D_8$, we may sort the reflections in D_8 into those that are in D_4 and those that are not. The representation $1++$ is described by functions even with respect to all reflections, and $1--$ by all functions odd with respect to all reflections. Similarly, $1+-$ functions are odd with respect to D_4 reflections and even with respect to all other reflections, while for $1-+$ functions the situation is reversed. The miniaturizations u_+ (for $1++$ or $1+-$ eigenfunctions) and u_- (for $1-+$ or $1--$ eigenfunctions) are again given by (5–3) and (5–4), where the $\pm$ signs alternate along the eight small octagons. We note that the representation type is preserved under miniaturization.

In this case there are three two-dimensional representations, denoted by $2_1, 2_2, 2_3$. In terms of complex-valued functions on the circle, 2_1 is spanned by $e^{\pm 2\pi i\theta/8}$, 2_2 is spanned by $e^{\pm 2\pi i 2\theta/8}$, and 2_3 is spanned by $e^{\pm 2\pi 3i\theta/8}$. If x, y, z denote any consecutive points on an eight-element orbit of D_8, then 2_1 functions satisfy

$$u(y) = \frac{\sqrt{2}}{2}(u(x) + u(z)), \tag{5–6}$$

2_2 functions satisfy

$$u(x) + u(z) = 0, \tag{5–7}$$

and 2_3 functions satisfy

$$u(y) = -\frac{\sqrt{2}}{2}(u(x) + u(z)). \tag{5–8}$$

The 2_1 and 2_3 representations have the property that restricted to D_4 they become the 2 representation. So if u, v are the basis described above, the miniaturizations u_2, v_2 are given in Figure 12. On the other hand, the restriction of 2_2 to D_4 splits into a direct sum of a $1+-$ and a $1-+$ representation. So we can choose a basis u, v such that

$$\rho_{\mathrm{H}} u = \rho_{\mathrm{V}} u = u = -\rho'_{\mathrm{D}} u = -\rho''_{\mathrm{D}} u,$$
$$-\rho_{\mathrm{H}} v = -\rho_{\mathrm{V}} v = v = \rho'_{\mathrm{D}} v = \rho''_{\mathrm{D}} v,$$

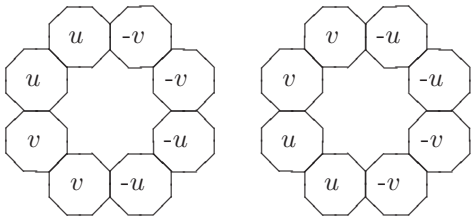

FIGURE 12. The miniaturizations (a) u_2 and (b) v_2 for a 2_1 or 2_3 eigenspace.

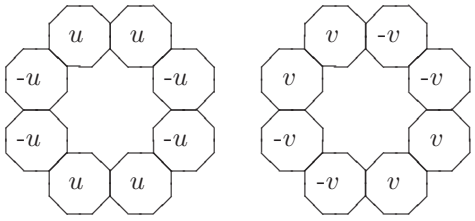

FIGURE 13. The miniaturizations (a) u_2' and (b) v_2' for a 2_2 eigenspace.

and the miniaturization u_2', v_2' is given in Figure 13. Again the representation type is preserved under miniaturization.

Some types of miniaturization on the pentagasket are described in [Adams et al. 03].

6. RANDOM CARPETS

For $j \in \mathbb{Z}$, $j > 1$, we partition the unit square into a grid of $j \times j$ smaller, equal-size squares of width $1/j$. We then randomly remove k of these smaller squares, where k is a small positive integer, and the result is our level-1 domain Ω_1. To produce Ω_2, we partition each square of width $1/j$ into a grid of $j \times j$ equal-size squares of width $1/j^2$, and we then randomly remove m squares of width $1/j^2$ from each square of width $1/j$. Iterating this process yields a sequence of nested compact domains $\{\Omega_m\}_{m=1}^{\infty}$, where Ω_m is a union of squares of side length j^{-m}. Matlab's `rand('state')` function, a modified version of Marsaglia's subtract-with-borrow algorithm, makes our random choices. The number generator's state is set according to the exact date and time of the computation, so that the generator's own state is essentially randomly determined. Also, to shorten FEM computation time we triangulate Ω_m with the four sides and two diagonals of each square of side length j^{-m}.

The problem we find with our FEM eigenvalue problem on these domains is connectivity. How can we guarantee that each Ω_m has only one path component? Also, if two squares are disjoint except at a common vertex, with no other squares in a neighborhood of that vertex, how can we avoid the problem we saw in Section 3? Recall that in this case, the spline space of our finite-element solver couples these squares at the common vertex. For simplicity we resolve both questions by choosing small k and altering the above algorithm so that this coupling problem is avoided, as follows. When we pass from Ω_m to Ω_{m+1}, we partition a square of side length j^{-m} into squares of side length j^{-m-1} and delete k of the smaller squares randomly. We then check whether this deletion process has produced the above coupling problem. If it has, then we go back and try again; otherwise, we move on to the next mth-level square, and so on. For k small enough, the algorithm terminates. Figure 14 shows a typical result of the above algorithm. Notice that we have only one path component.

Now we study our spectral information with the eigenvalue-counting function $N : [0, \infty) \to \mathbb{Z}$, where $N(x)$ is the number of nonnegative eigenvalues less than or equal to x. Then we examine the Weyl ratio

$$W(x) = \frac{N(x)}{x^{\alpha}}, \tag{6–1}$$

where x^{α} is an approximate asymptotic bound for $N(x)$, i.e., we choose $\alpha \in \mathbb{R}$ such that $N(x) \sim x^{\alpha}$ in accordance with the experimental data. So, finding α corresponds to finding the slope of a linear approximation of $N(x)$ on a log-log plot. In fact, since we are dealing with domains

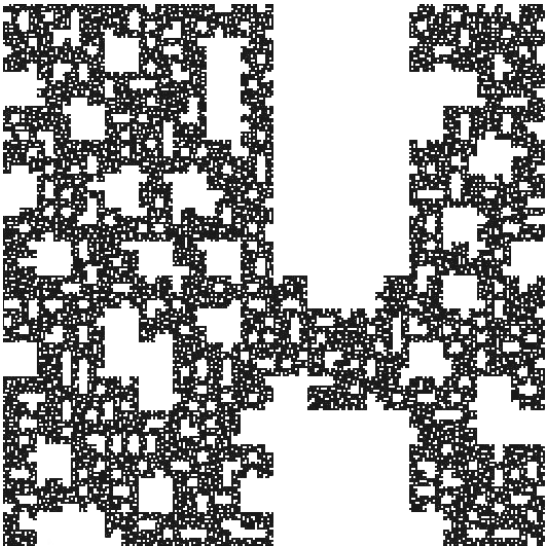

FIGURE 14. Level-4 domain Ω_4 for $j = 4$, $k = 3$.

in the plane, the Weyl asymptotic law implies that $\alpha = 1$ is the correct value as $x \to \infty$. The point is that we truncate our computations well before we reach the region where this asymptotic behavior is approximated, so we observe values of α considerably smaller than 1.

In our first example, we let $j = 4$ and $k = 2$ and run our algorithm up to level 4 to get $\{\Omega_i\}_{i=1}^4$, where Ω_4 is the upper left carpet in Figure 15. From this initial carpet, we can restart our algorithm three separate times, beginning at Ω_i once for each $i = 1, 2, 3$. We then end the algorithm again at level 4 and we call the resulting (level-4) carpet that was started at Ω_i the bifurcation of Ω_4 at level $i + 1$. The carpets are shown in Figure 15 and the eigenvalue data in Tables 18 and 19. Next, we let $j = 4$ and $k = 3$ and do the same bifurcation study. The carpets are shown in Figure 17 and the eigenvalue data in Tables 20 and 21.

Finally, we fix $j = 4$ and vary k on different levels so that at level 1 we set $k = 2$, at level 2 we set $k = 3$, etc. A similar procedure for gaskets rather than carpets is discussed in [Drenning and Strichartz 08]. Our sequence of k values for the carpet in Figure 19 is $k = \{2, 3, 2, 3, 2\}$. The eigenvalue data appear in Tables 22 and 23. The level-to-level eigenvalue ratios in Table 22 appear roughly to alternate between the same ratios in Tables 20 and 18. This is the strongest evidence that the geometry of the domain at different scales is reflected in the spectrum of the Laplacian. Such a correlation is more striking in [Drenning and Strichartz 08], but the fractals there have a more coherent structure.

The Weyl ratios of our first example (where $j = 4$ and $k = 2$) appear in Figure 16. We now look closely at the agreement of the graph of the original carpet to each individual bifurcation. We see that the original agrees with the bifurcation at level 4 up to about $x = 300$, the original agrees with that at level 3 up to around $x = 65$, and it agrees with the level-2 bifurcation up to about $x = 25$. In our second example (where $j = 4$ and $k = 4$) we find the Weyl ratios in Figure 18. We do the same comparison. The original agrees with the level-4 bifurcation to around $x = 150$, it agrees with the level-3 bifurcation up to approximately $x = 30$, and it agrees with the level-2 bifurcation to approximately $x = 10$. In other words, the added detail at finer resolutions has only a minimal effect on some initial segment of the spectrum. This is consistent with results in [Drenning and Strichartz 08]. Our final example's Weyl ratios (where $j = 4$ and $k = \{2, 3, 2, 3, 2\}$) are found in Figure 20.

For further comparison of the Weyl ratios, we show those from another trial with $j = 4$ and $k = 2$, and those from another trial with $j = 4$ and $k = 3$. The carpets for the new $j = 4$, $k = 2$ trial appear in Figure 21 with Weyl ratios in Figure 22, while the carpets for the new $j = 4$, $k = 3$ trial appear in Figure 23 with Weyl ratios in Figure 24. It is clear that different random choices in the construction make a big difference in the spectrum. We leave to the future the problem of formulating precise conjectures concerning the spectra of different random carpets.

	Original carpet				Bif. level 4	Bif. level 3		Bif. level 2			Orig. ratios $\lambda_n^{j+1}/\lambda_n^j$		
Level	1	2	3	4	4	3	4	2	3	4			
Refinement	2	1	0	0	0	0	0	1	0	0			
n													
1	5.580	4.524	3.961	3.331	3.349	3.885	3.248	5.011	4.393	3.689	0.811	0.875	0.841
2	7.666	6.734	5.914	5.008	5.009	5.963	4.990	6.384	5.528	4.639	0.878	0.878	0.847
3	18.031	15.575	13.671	11.556	11.543	13.514	11.311	15.597	13.664	11.478	0.864	0.878	0.845
4	31.079	24.699	21.630	18.234	18.269	21.733	18.259	27.549	24.099	20.091	0.795	0.876	0.843
5	40.933	35.373	31.097	26.152	25.983	31.230	26.123	35.484	31.262	26.392	0.864	0.879	0.841
6	46.442	37.463	32.776	27.549	27.640	32.326	27.255	38.315	33.722	28.249	0.807	0.875	0.841
7	49.757	41.840	36.519	30.975	30.850	36.427	30.614	45.424	39.840	33.521	0.841	0.873	0.848
8	72.354	62.389	54.211	45.450	45.767	54.977	45.924	56.607	49.171	41.245	0.862	0.869	0.838
9	88.309	74.938	65.259	54.360	54.880	65.444	54.860	70.649	61.489	51.576	0.849	0.871	0.833
10	96.790	77.384	65.694	55.376	55.582	66.288	54.919	74.244	63.358	53.123	0.799	0.849	0.843

TABLE 18. Carpet bifurcation unnormalized eigenvalues for $j = 4$, $k = 2$.

	Original carpet				Bif. level 4	Bif. level 3		Bif. level 2		
Level	1	2	3	4	4	3	4	2	3	4
Refinement	2	1	0	0	0	0	0	1	0	0
n										
1	1.000	1.000	1.000	1.000	1.000	1.000	1.000	1.000	1.000	1.000
2	1.374	1.489	1.493	1.503	1.496	1.535	1.536	1.274	1.258	1.257
3	3.231	3.443	3.452	3.469	3.447	3.479	3.482	3.113	3.110	3.111
4	5.570	5.460	5.461	5.473	5.455	5.595	5.621	5.498	5.485	5.445
5	7.336	7.819	7.852	7.850	7.758	8.039	8.042	7.082	7.116	7.153
6	8.323	8.281	8.276	8.270	8.253	8.322	8.391	7.647	7.676	7.657
7	8.917	9.249	9.221	9.298	9.211	9.377	9.425	9.066	9.068	9.086
8	12.967	13.791	13.688	13.643	13.665	14.152	14.138	11.297	11.192	11.179
9	15.826	16.565	16.477	16.318	16.387	16.847	16.889	14.100	13.996	13.979
10	17.346	17.106	16.587	16.623	16.596	17.064	16.907	14.817	14.421	14.399

TABLE 19. Carpet bifurcation normalized eigenvalues for $j = 4$, $k = 2$.

	Original carpet				Bif. level 4	Bif. level 3		Bif. level 2			Orig. ratios $\lambda_n^{j+1}/\lambda_n^j$		
Level	1	2	3	4	4	3	4	2	3	4			
Refinement	2	1	0	0	0	0	0	1	0	0			
n													
1	7.092	4.504	3.375	2.426	2.445	3.493	2.631	6.127	4.897	3.695	0.635	0.749	0.719
2	11.728	8.197	6.565	4.765	4.809	6.560	4.906	9.482	7.315	5.436	0.699	0.801	0.726
3	24.546	15.759	12.132	9.007	8.969	12.351	9.397	21.222	16.397	12.210	0.642	0.770	0.742
4	30.185	18.800	15.634	11.511	11.431	15.081	11.247	23.081	17.654	13.228	0.623	0.832	0.736
5	42.518	27.342	22.736	16.597	17.156	21.355	15.651	35.771	28.705	21.604	0.643	0.832	0.730
6	58.544	39.332	31.633	23.474	23.415	29.450	21.692	42.024	34.860	25.822	0.672	0.804	0.742
7	61.533	48.008	39.592	29.343	28.460	37.253	26.997	51.343	38.677	28.823	0.780	0.825	0.741
8	77.637	55.316	44.954	33.046	33.484	43.576	33.038	62.867	47.085	35.453	0.712	0.813	0.735
9	83.257	65.486	50.292	37.106	37.063	50.448	38.068	69.055	53.226	39.577	0.787	0.768	0.738
10	104.768	73.075	55.186	39.936	40.286	56.936	42.856	82.013	62.297	45.968	0.697	0.755	0.724

TABLE 20. Carpet bifurcation unnormalized eigenvalues for $j = 4$, $k = 3$.

	Original carpet				Bif. level 4	Bif. level 3		Bif. level 2		
Level	1	2	3	4	4	3	4	2	3	4
Refinement	2	1	0	0	0	0	0	1	0	0
n										
1	1.000	1.000	1.000	1.000	1.000	1.000	1.000	1.000	1.000	1.000
2	1.654	1.820	1.945	1.964	1.967	1.878	1.865	1.548	1.494	1.471
3	3.461	3.499	3.595	3.712	3.668	3.536	3.572	3.464	3.349	3.305
4	4.256	4.174	4.633	4.744	4.675	4.317	4.275	3.767	3.605	3.580
5	5.995	6.071	6.737	6.840	7.016	6.113	5.950	5.839	5.862	5.847
6	8.255	8.732	9.374	9.674	9.576	8.431	8.246	6.859	7.119	6.989
7	8.676	10.659	11.732	12.093	11.640	10.665	10.263	8.380	7.899	7.801
8	10.947	12.281	13.321	13.619	13.694	12.475	12.559	10.262	9.616	9.595
9	11.740	14.539	14.903	15.292	15.158	14.442	14.471	11.272	10.870	10.712
10	14.773	16.224	16.353	16.459	16.476	16.300	16.291	13.387	12.723	12.441

TABLE 21. Carpet bifurcation normalized eigenvalues for $j = 4$, $k = 3$.

	Eigenvalue data					**Ratios $\lambda_n^{j+1}/\lambda_n^j$**			
Level	1	2	3	4	5	$j=1$	$j=2$	$j=3$	$j=4$
Refinement	2	1	0	0	0				
n									
1	7.812	5.846	5.041	3.855	3.160	0.748	0.862	0.765	0.820
2	11.846	8.843	7.739	5.918	4.865	0.746	0.875	0.765	0.822
3	16.892	11.188	9.621	7.327	6.019	0.662	0.860	0.762	0.821
4	31.783	21.564	18.685	14.339	11.813	0.678	0.867	0.767	0.824
5	38.849	27.674	24.037	18.351	15.056	0.712	0.869	0.763	0.820
6	44.579	33.739	28.815	21.870	17.953	0.757	0.854	0.759	0.821
7	66.179	53.267	45.651	34.817	28.614	0.805	0.857	0.763	0.822
8	79.132	57.301	50.164	38.328	31.538	0.724	0.875	0.764	0.823
9	91.235	64.613	55.715	42.305	34.727	0.708	0.862	0.759	0.821
10	93.671	71.615	60.579	45.932	37.773	0.765	0.846	0.758	0.822

TABLE 22. Carpet mixed unnormalized eigenvalues and ratios, $\{2, 3, 2, 3, 2\}$.

Level	1	2	3	4	5
Refinement	2	1	0	0	0
n					
1	1.000	1.000	1.000	1.000	1.000
2	1.516	1.513	1.535	1.535	1.540
3	2.162	1.914	1.908	1.901	1.905
4	4.068	3.689	3.707	3.720	3.739
5	4.973	4.734	4.768	4.761	4.765
6	5.706	5.771	5.716	5.673	5.681
7	8.471	9.112	9.056	9.032	9.055
8	10.129	9.802	9.951	9.943	9.981
9	11.679	11.052	11.052	10.975	10.990
10	11.991	12.250	12.017	11.916	11.954

TABLE 23. Carpet mixed normalized eigenvalues $\{2, 3, 2, 3, 2\}$.

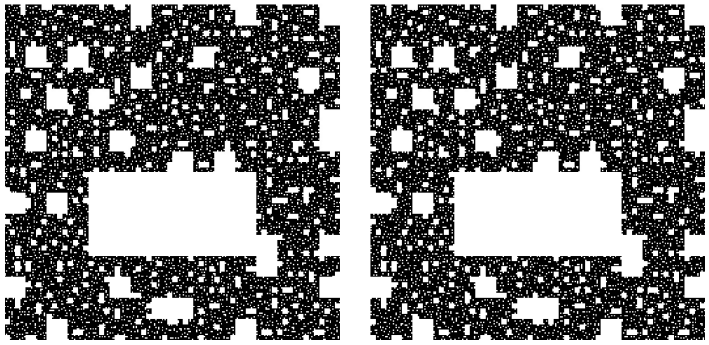

Original Carpet Bifurcation at Level 4

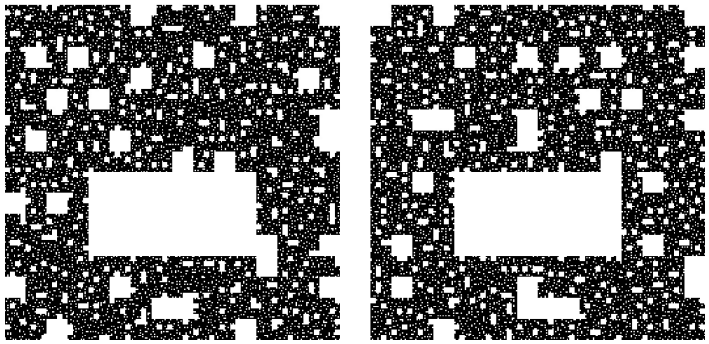

Bifurcation at Level 3 Bifurcation at Level 2

FIGURE 15. Carpet bifurcations Ω_4 for $j = 4$, $k = 2$.

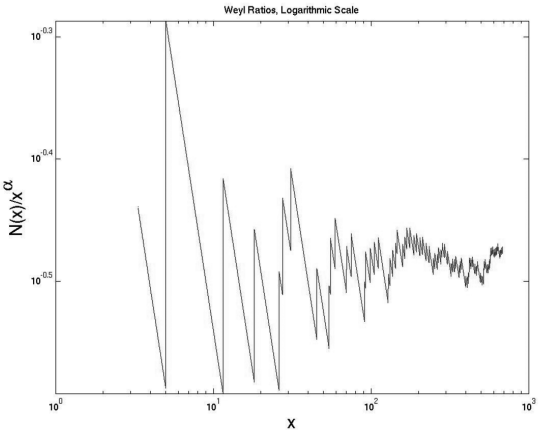

Original Carpet, $\alpha = .84032$

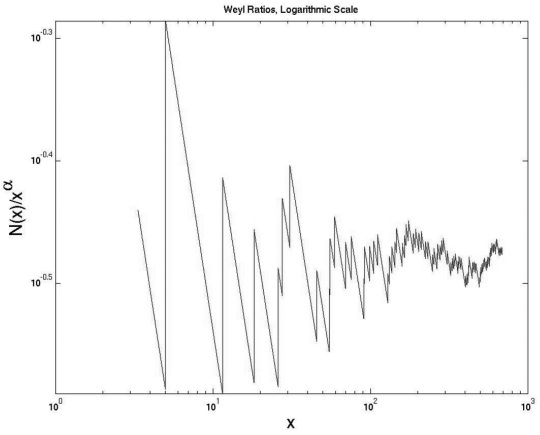

Bifurcation at Level 4, $\alpha = .83853$

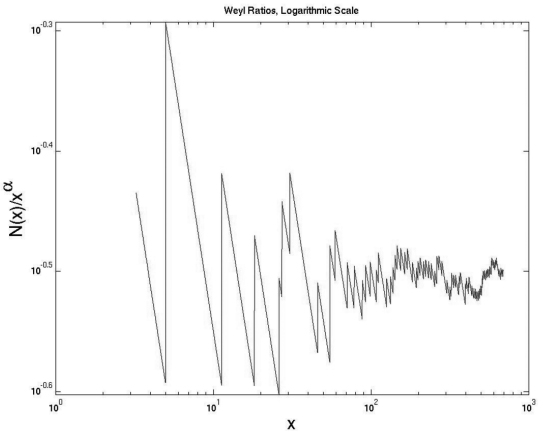

Bifurcation at Level 3, $\alpha = 0.85007$

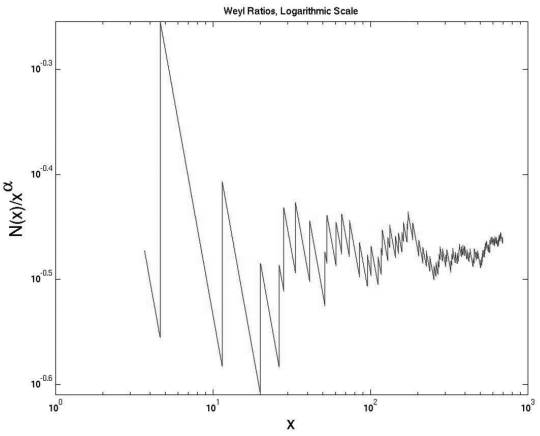

Bifurcation at Level 2, $\alpha = 0.83383$

FIGURE 16. Weyl ratios for $j = 4$, $k = 2$.

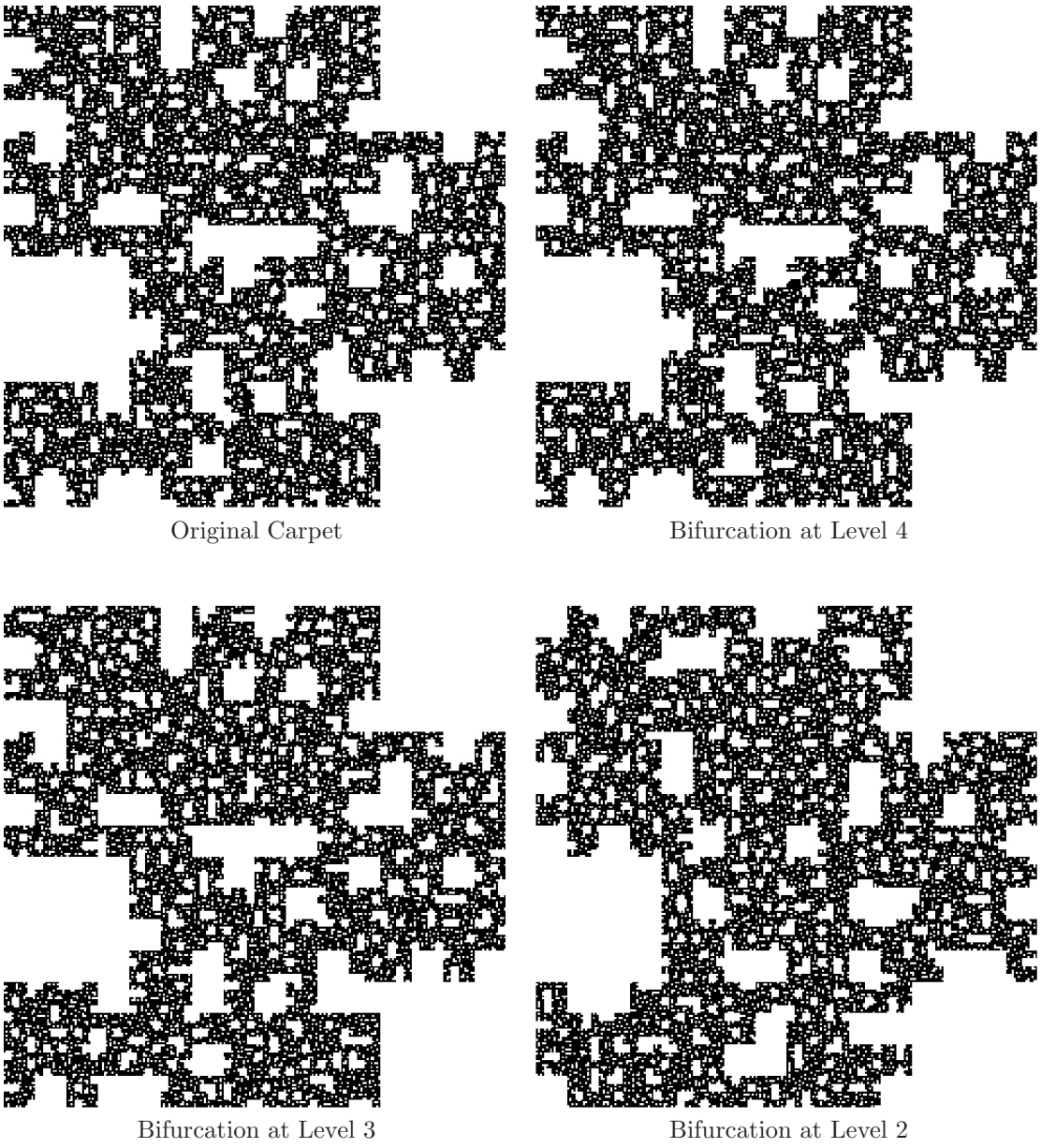

FIGURE 17. Carpet bifurcations Ω_4 for $j = 4$, $k = 3$.

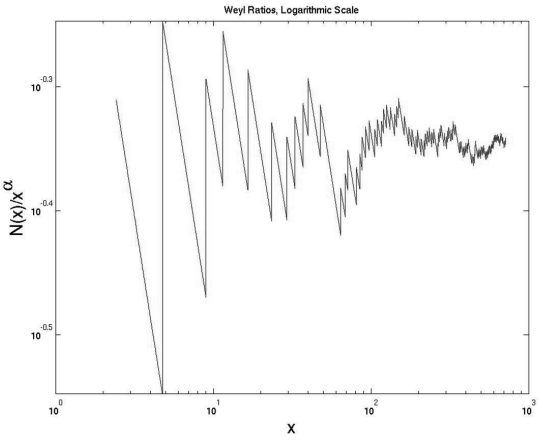

Original Carpet, $\alpha = .80788$

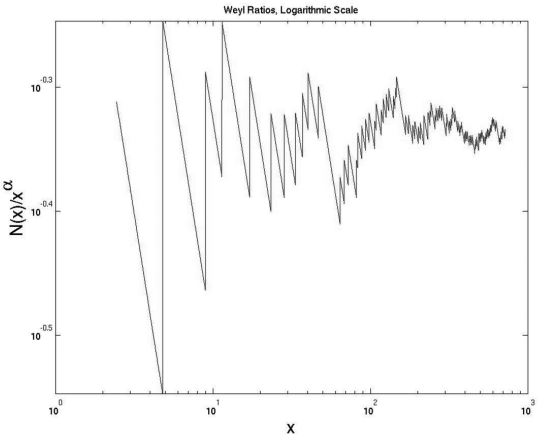

Bifurcation at Level 4, $\alpha = .80253$

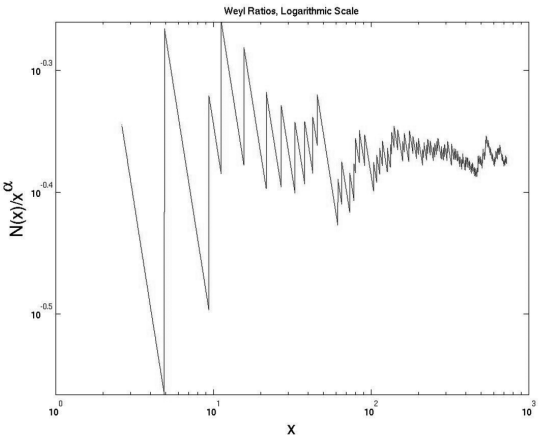

Bifurcation at Level 3, $\alpha = .82004$

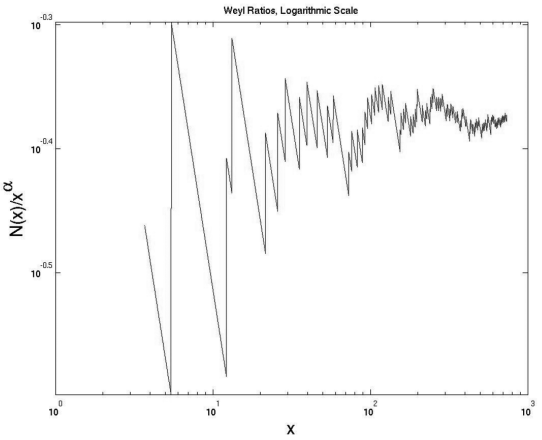

Bifurcation at Level 2, $\alpha = .81408$

FIGURE 18. Weyl ratios for $j = 4$, $k = 3$.

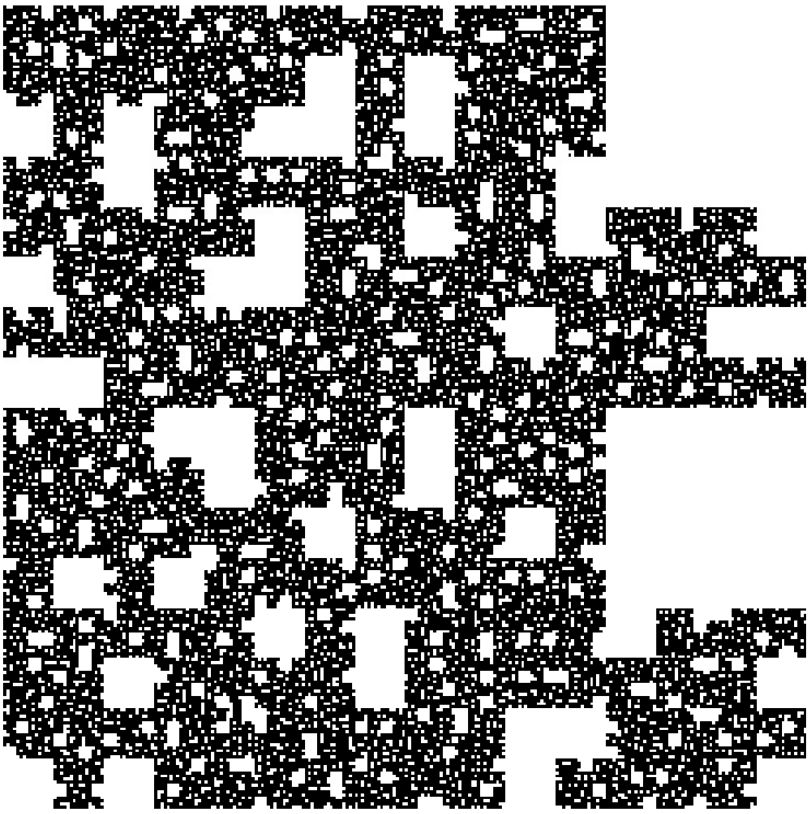

FIGURE 19. Level-4 domain Ω_4 for $j = 4$, $D : 2, 3, 2, 3, 2$.

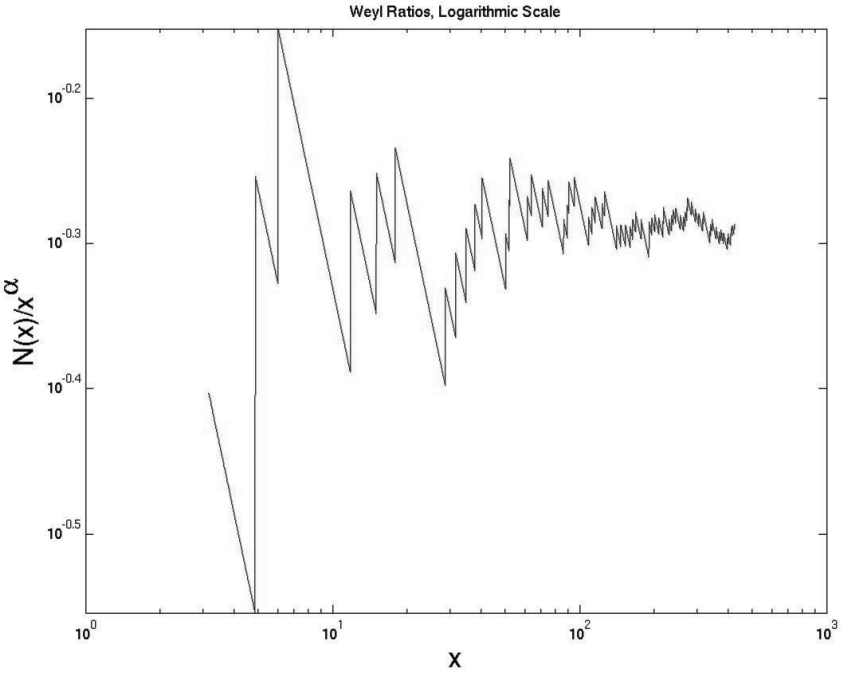

FIGURE 20. Weyl ratios for $j = 4$, $k = \{2, 3, 2, 3, 2\}$, level 5 carpet, $\alpha = 0.8071$.

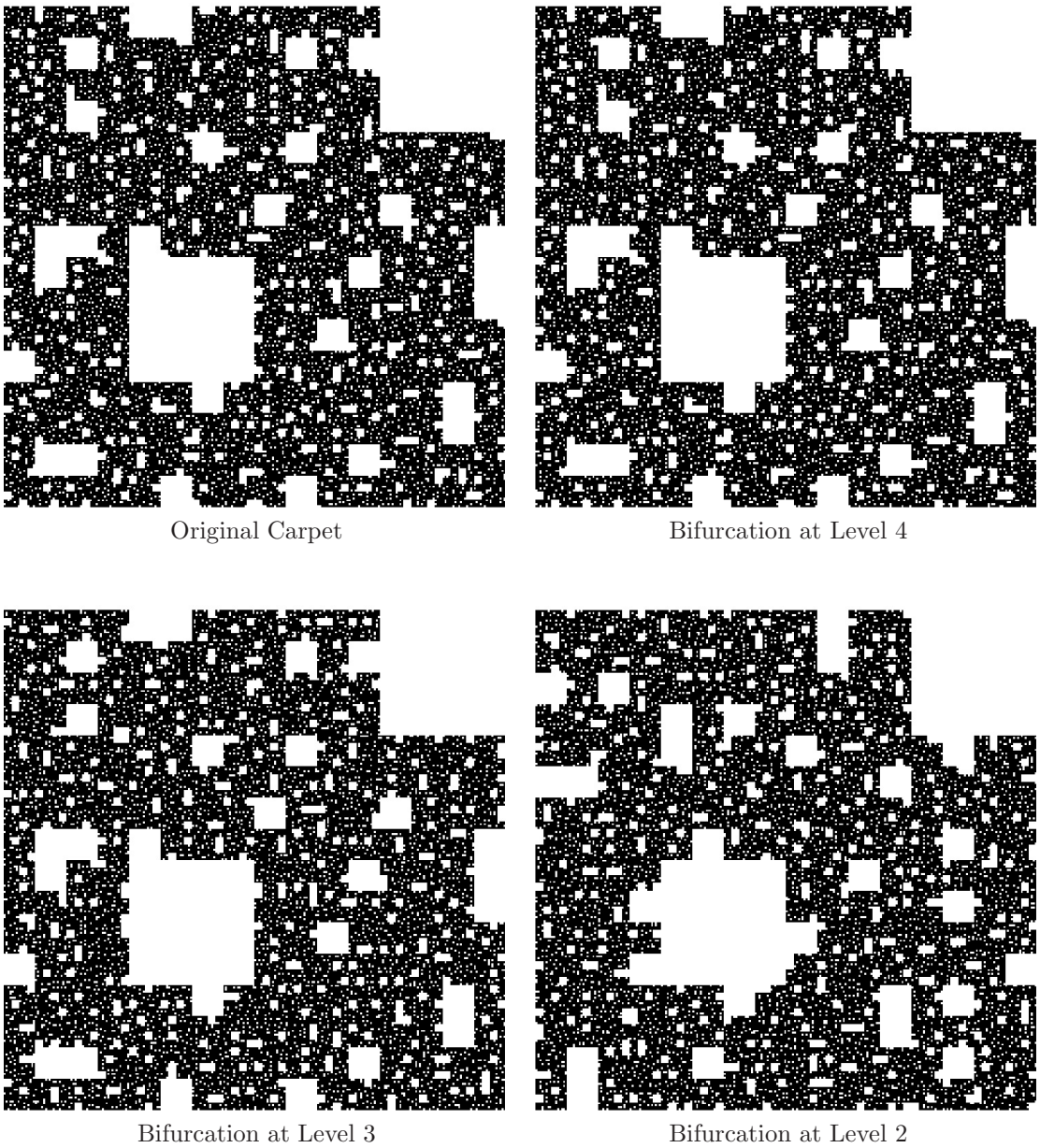

Original Carpet | Bifurcation at Level 4

Bifurcation at Level 3 | Bifurcation at Level 2

FIGURE 21. Carpet bifurcations Ω_4 for $j = 4$, $k = 2$.

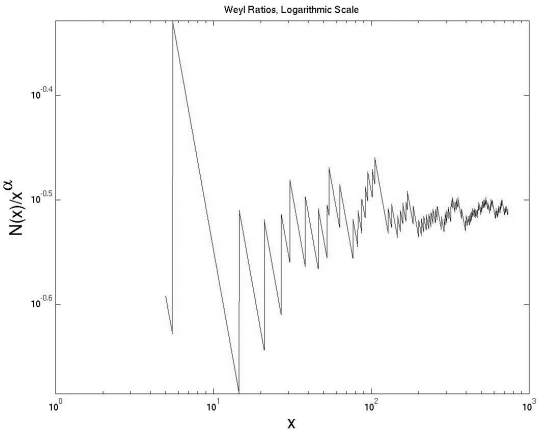

Original Carpet, $\alpha = .84747$

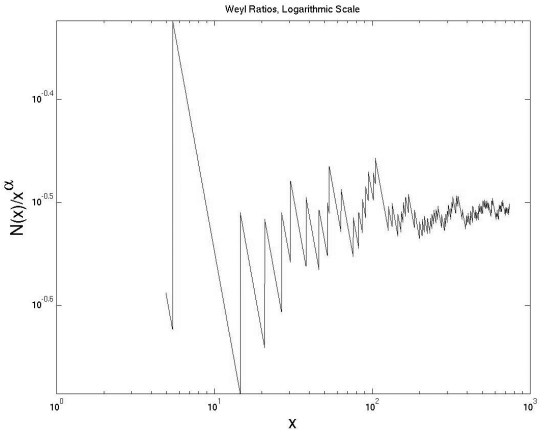

Bifurcation at Level 4, $\alpha = .84753$

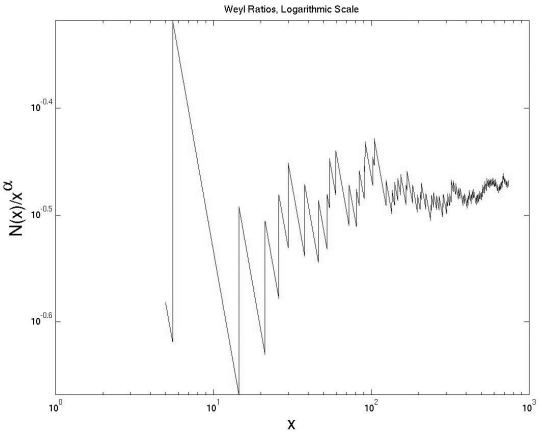

Bifurcation at Level 3, $\alpha = .83368$

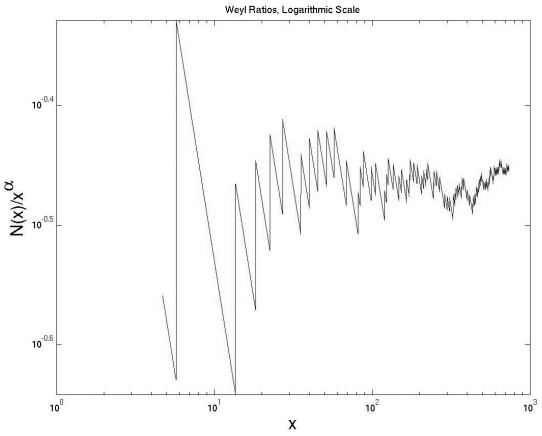

Bifurcation at Level 2, $\alpha = .83019$

FIGURE 22. Weyl ratios for $j = 4$, $k = 2$.

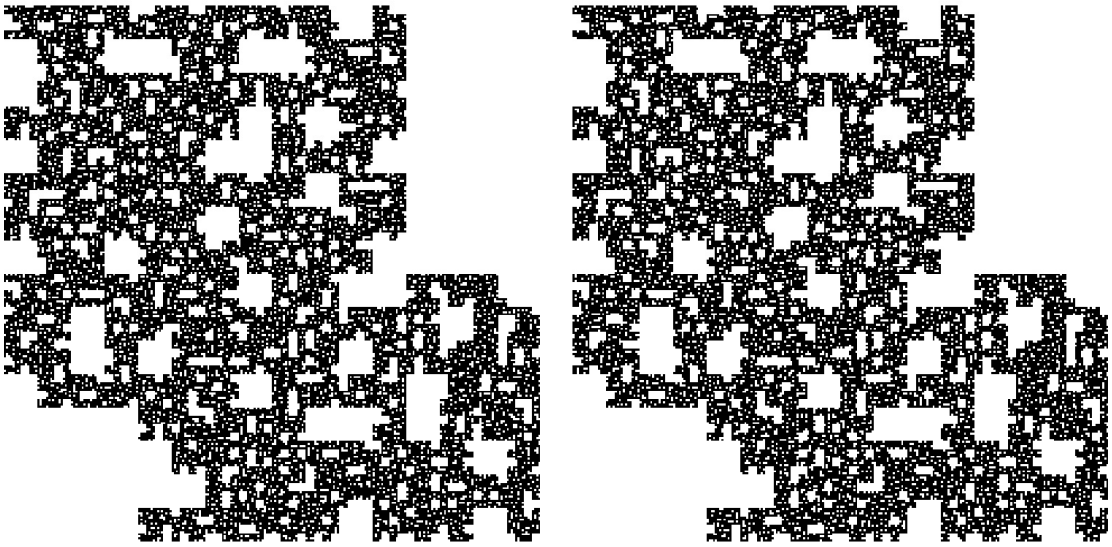

Original Carpet

Bifurcation at Level 4

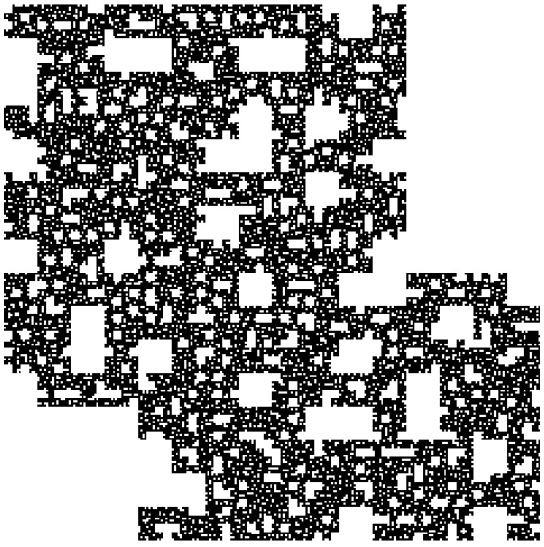

Bifurcation at Level 3

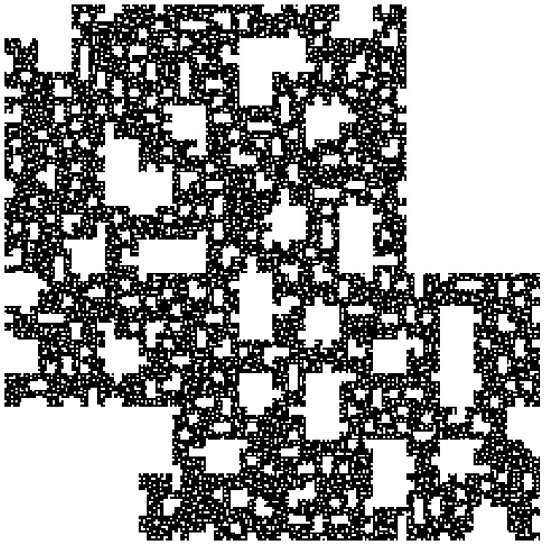

Bifurcation at Level 2

FIGURE 23. Carpet bifurcations Ω_4 for $j = 4$, $k = 3$.

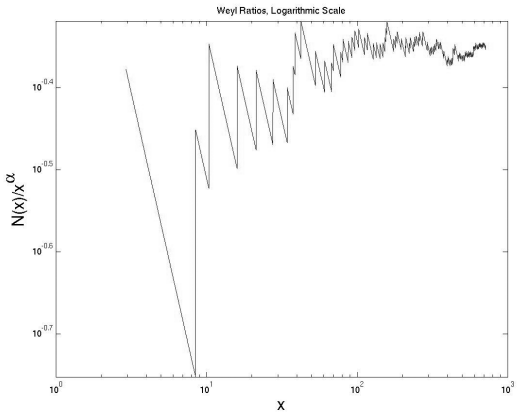

Original Carpet, $\alpha = .81013$

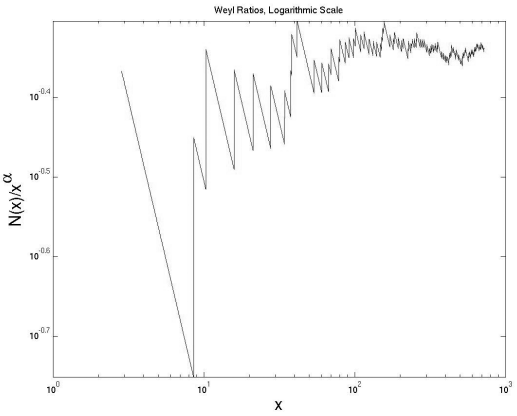

Bifurcation at Level 4, $\alpha = .80544$

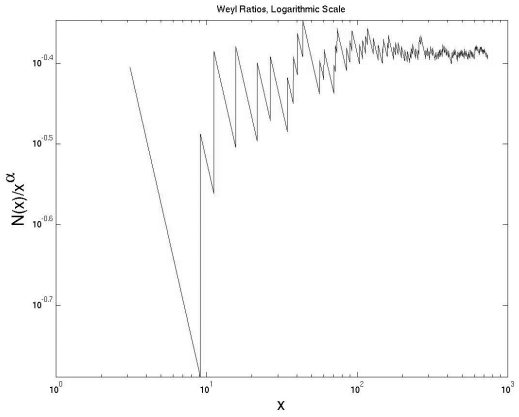

Bifurcation at Level 3, $\alpha = .82086$

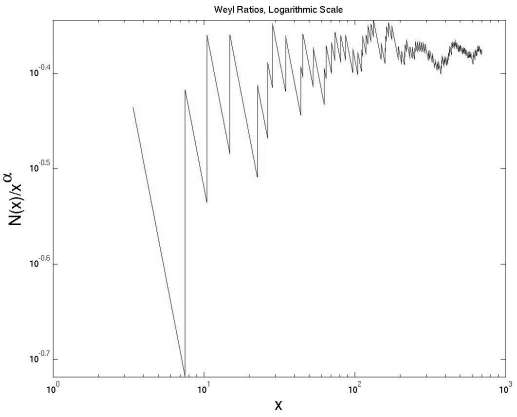

Bifurcation at Level 2, $\alpha = .81975$

FIGURE 24. Weyl ratios for $j = 4$, $k = 3$.

ACKNOWLEDGMENTS

We are grateful to Stacey Goff, who contributed to the numerical experiments. The first and second authors were supported by the National Science Foundation through the Research Experiences for Undergraduates (REU) program at Cornell University. The third author was supported in part by the National Science Foundation, Grant DMS 0652440.

REFERENCES

[Adams et al. 03] Bryant Adams, S. Alex Smith, Robert S. Strichartz, and Alexander Teplyaev. "The Spectrum of the Laplacian on the Pentagasket." In *Fractals in Graz 2001*, Trends Math., pp. 1–24. Basel: Birkhäuser, 2003.

[Barlow 95] Martin T. Barlow. "Diffusions on Fractals." In *Lectures on Probability Theory and Statistics (Saint-Flour, 1995)*, Lecture Notes in Math. 1690, pp. 1–121. Berlin: Springer, 1998.

[Barlow and Bass 89] M. T. Barlow and R. F. Bass. "The Construction of Brownian Motion on the Sierpiński Carpet." *Ann. Inst. H. Poincaré Probab. Statist.* 25 (1989), 225–257.

[Barlow and Bass 99] M. T. Barlow, R. F. Bass. "Brownian Motion and Harmonic Analysis on Sierpiński Carpets." *Canad. J. Math.* 51:4 (1999), 673–744.

[Barlow et al. 90] M. T. Barlow, R. F. Bass, and J. D. Sherwood. "Resistance and Spectral Dimension of Sierpiński Carpets." *J. Phys. A* 23:6 (1990), L253–L258.

[Barlow et al. 08] M. T. Barlow, R. F. Bass, T. Kumagai, and A. Teplyaev. "Uniqueness of Brownian Motion on Sierpiński Carpets." Preprint, 2008, arXiv:0812.1802v2.

[Blasiak et al. 08] Anna Blasiak, Robert S. Strichartz, and Baris Evren Ugurcan. "Spectra of Self-Similar Laplacians on the Sierpiński Gasket with Twists." *Fractals* 16:1 (2008), 43–68.

[Broman and Camia 08] Erik I. Broman and Federico Camia. 'Large-N Limit of Crossing Probabilities, Discontinuity, and Asymptotic Behavior of Threshold Values in Mandelbrot's Fractal Percolation Process." *Electron. J. Probab.* 13:3 (2008), 980–999.

[Chayes et al. 88] J. T. Chayes, L. Chayes, and R. Durrett. "Connectivity Properties of Mandelbrot's Percolation Process." *Probab. Theory Related Fields* 77:3 (1988), 307–324.

[Colin de Verdière 98] Yves Colin de Verdière. *Spectres de graphes, Cours Spécialisés [Specialized Courses]*, vol. 4. Paris: Société Mathématique de France, 1998.

[Dalrymple et al. 99] Kyalle Dalrymple, Robert S. Strichartz, and Jade P. Vinson. "Fractal Differential Equations on the Sierpiński Gasket." *J. Fourier Anal. Appl.* 5:2–3 (1999), 203–284.

[Dodziuk and Patodi 76] J. Dodziuk and V. K. Patodi. "Riemannian Structures and Triangulations of Manifolds." *J. Indian Math. Soc. (N.S.)* 40 (1976), 1–52.

[Drenning and Strichartz 08] Shawn Drenning and Robert S. Strichartz. "Spectral Decimation on Hambly's Homogeneous Hierarchical Gaskets." Preprint, 2008.

[Heilman and Strichartz 10] Steven M. Heilman and Robert S. Strichartz. "Localized Eigenfunctions: Here You See Them, There You Don't." (to appear), *Notices of the AMS*, arXiv:0909.0783v1.

[Kigami 01] Jun Kigami. *Analysis on Fractals*, Cambridge Tracts in Mathematics 143. Cambridge, UK: Cambridge University Press, 2001.

[Kuchment and Zeng 01] Peter Kuchment and Hongbiao Zeng. "Convergence of Spectra of Mesoscopic Systems Collapsing onto a Graph." *J. Math. Anal. Appl.* 258 (2001), 671–700.

[Strichartz 67] Robert S. Strichartz. "Multipliers on Fractional Sobolev Spaces." *J. Math. Mech.* 16 (1967), 1031–1060.

[Strichartz 99] Robert S. Strichartz. "Analysis on Fractals." *Notices Amer. Math. Soc.* 46:10 (1999), 1199–1208.

[Strichartz 03] Robert S. Strichartz, "Fractafolds Based on the Sierpiński Gasket and Their Spectra." *Trans. Amer. Math. Soc.* 355:10 (2003), 4019–4043.

[Strichartz 06] Robert S. Strichartz. *Differential Equations on Fractals: A Tutorial*. Princeton: Princeton University Press, 2006.

Tyrus Berry, Department of Mathematical Sciences, George Mason University, Fairfax, VA 22030 (tberry@gmu.edu)

Steven M. Heilman, Courant Institute of Mathematical Sciences, New York University, New York, NY 10012-1185 (smh82@cornell.edu)

Robert S. Strichartz, Department of Mathematics, Cornell University, Ithaca, NY 14850-4201 (str@math.cornell.edu)

Received June 9, 2008; accepted February 4, 2009.